NASA/CR-2005-213272

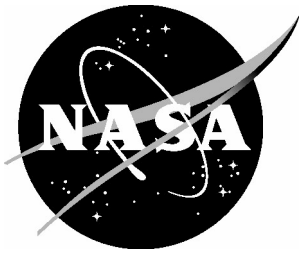

Strain Sensitivity in Single Walled Carbon Nanotubes for Multifunctional Materials

Jan M. Smits, VI
Lockheed Martin Space Operations, Hampton, Virginia

July 2005

The NASA STI Program Office . . . in Profile

Since its founding, NASA has been dedicated to the advancement of aeronautics and space science. The NASA Scientific and Technical Information (STI) Program Office plays a key part in helping NASA maintain this important role.

The NASA STI Program Office is operated by Langley Research Center, the lead center for NASA's scientific and technical information. The NASA STI Program Office provides access to the NASA STI Database, the largest collection of aeronautical and space science STI in the world. The Program Office is also NASA's institutional mechanism for disseminating the results of its research and development activities. These results are published by NASA in the NASA STI Report Series, which includes the following report types:

- TECHNICAL PUBLICATION. Reports of completed research or a major significant phase of research that present the results of NASA programs and include extensive data or theoretical analysis. Includes compilations of significant scientific and technical data and information deemed to be of continuing reference value. NASA counterpart of peer-reviewed formal professional papers, but having less stringent limitations on manuscript length and extent of graphic presentations.

- TECHNICAL MEMORANDUM. Scientific and technical findings that are preliminary or of specialized interest, e.g., quick release reports, working papers, and bibliographies that contain minimal annotation. Does not contain extensive analysis.

- CONTRACTOR REPORT. Scientific and technical findings by NASA-sponsored contractors and grantees.

- CONFERENCE PUBLICATION. Collected papers from scientific and technical conferences, symposia, seminars, or other meetings sponsored or co-sponsored by NASA.

- SPECIAL PUBLICATION. Scientific, technical, or historical information from NASA programs, projects, and missions, often concerned with subjects having substantial public interest.

- TECHNICAL TRANSLATION. English-language translations of foreign scientific and technical material pertinent to NASA's mission.

Specialized services that complement the STI Program Office's diverse offerings include creating custom thesauri, building customized databases, organizing and publishing research results ... even providing videos.

For more information about the NASA STI Program Office, see the following:

- Access the NASA STI Program Home Page at ***http://www.sti.nasa.gov***

- E-mail your question via the Internet to help@sti.nasa.gov

- Fax your question to the NASA STI Help Desk at (301) 621-0134

- Phone the NASA STI Help Desk at (301) 621-0390

- Write to:
  NASA STI Help Desk
  NASA Center for AeroSpace Information
  7121 Standard Drive
  Hanover, MD 21076-1320

NASA/CR-2005-213272

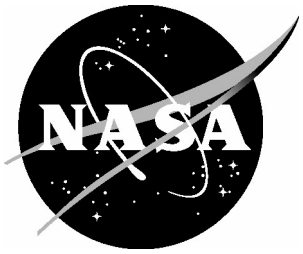

Strain Sensitivity in Single Walled Carbon Nanotubes for Multifunctional Materials

Jan M. Smits, VI
Lockheed Martin Space Operations, Hampton, Virginia

National Aeronautics and
Space Administration

Langley Research Center
Hampton, Virginia 23681-2199

Prepared for Langley Research Center
under Contract NAS1-00135

July 2005

Available from:

NASA Center for AeroSpace Information (CASI)
7121 Standard Drive
Hanover, MD 21076-1320
(301) 621-0390

National Technical Information Service (NTIS)
5285 Port Royal Road
Springfield, VA 22161-2171
(703) 605-6000

Abstract

Single walled carbon nanotubes represent the future of structural aerospace vehicle systems due to their unparalleled strength characteristics and demonstrated multifunctionality. This multifunctionality rises from the CNT's unique capabilities for both metallic and semiconducting electron transport, electron spin polarizability, and band gap modulation under strain. By incorporating the use of electric field alignment and various lithography techniques, a single wall carbon nanotube (SWNT) test bed for measurement of conductivity/strain relationships has been developed. Nanotubes are deposited at specified locations through dielectrophoresis. The circuit is designed such that the central, current carrying section of the nanotube is exposed to enable atomic force microscopy and manipulation *in situ* while the transport properties of the junction are monitored. Studies of in-plane strains in the SWNTs produced through the use of the Nanomanipulator® haptic feedback atomic force microscope (AFM) system are discussed. By applying this methodology to sensor development a flexible single wall carbon nanotube (SWNT) based strain sensitive device has been developed. Nanotubes are deposited at specified locations on a polyimide substrate through dielectrophoresis. Studies of tensile testing of the flexible SWNT device vs conductivity are also presented. Future embodiments of such a device lead to CNT based multifunctional structural systems. The purpose of the research described in the current thesis is to investigate the possibility of using single walled HiPCO (high-pressure carbon monoxide) carbon nanotubes as strain sensing agents to be used in a multi-functional materials system. By demonstrating this feasibility further steps can be taken toward the advancement of future integrated structural health monitoring systems.

Contents

List of Figures

List of Acronyms

ACS	American Chemical Society
AFM	Atomic Force Microscope
APTES	3-Aminopropyltriethoxysilane
CAD	Computer Aided Design
CNT	Carbon Nanotube
CVD	Chemical Vapor Deposition
DEP	Dielectrophoresis
FEM	Finite Element Model
HF	Hydrofluoric Acid
HiPCO	High Pressure Carbon Monoxide (CNT growth Method)
IPA	Isopropanol
NPGS	Nanometer Pattern Generation System
PMMA	Poly(methyl methacrylate) - (electron beam resist)
RTD	Resistive Temperature Device
SAM	Self Assembled Monolayer
SEM	Scanning Electron Microscope
SPM	Scanning Probe Microscope
SQUID	Superconducting Quantum Interface Device
SWCNT	Single-Walled Carbon Nanotube
TMS	Trimethylsilyl
UV	Ultraviolet
ZIF	Zero Insertion Force

Chapter 1: Introduction

1.1 Background

In the early 1990's a material with extraordinary strength and transport properties was discovered that is now shaping the future of aerospace materials systems. Carbon nanotubes (CNTs), first observed by Sumio Iijima in Japan in 1991, come in two basic varieties, single-walled and multiwalled. Single walled CNTs consist of a single atomic layer graphene sheet rolled seamlessly into a tube structure, while multiwalled CNTs are several graphene sheets rolled into concentric tubes. Single walled carbon nanotubes (SWCNTs) are most often found to be less than 2 nm in diameter with length / width ratios as high as $10^4 – 10^5$ [1], and hence are considered one-dimensional. Their electronic properties may be either metallic or semiconducting depending on their chirality (the angle at which the tube is rolled with respect to the lattice axis) given by a chiral vector (n, m) which also defines the diameter of the tube. When n-m=3k, where k is a nonzero integer, the tubes are conductive or are semiconductors with zero bandgap. The different species of SWCNTs include armchair nanotubes which are metallic with m = n, and zigzag tubes having m=0. Any other configuration is referred to as chiral. This is illustrated in figure 1.1 along with several examples of different CNTs.

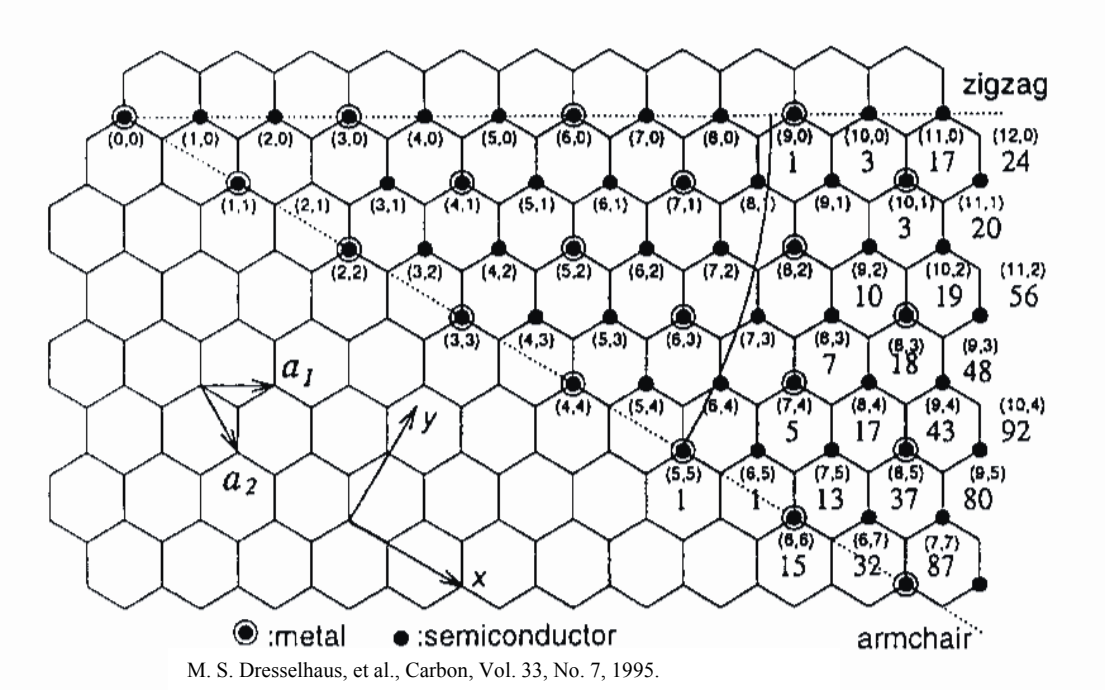

M. S. Dresselhaus, et al., Carbon, Vol. 33, No. 7, 1995.

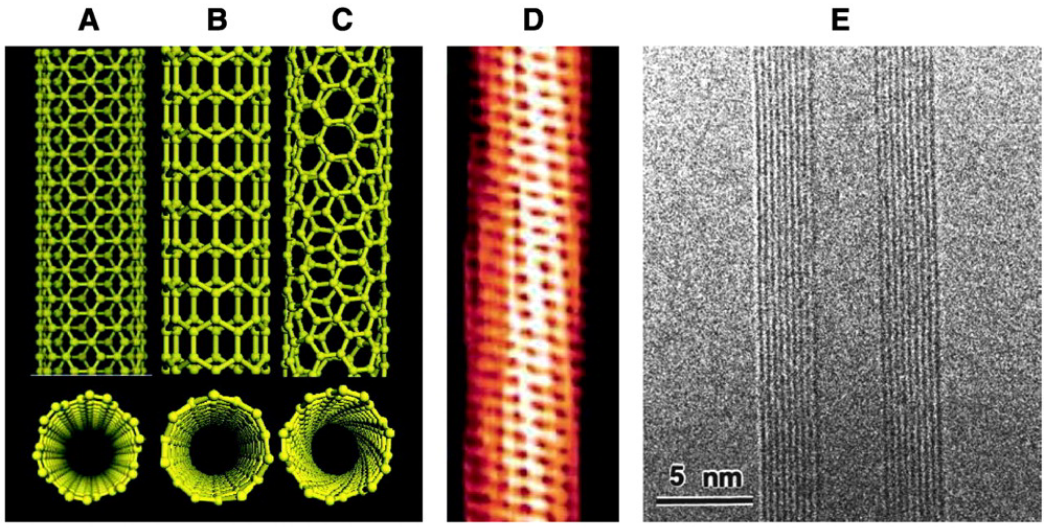

R.H. Baoughman et al. – "The Route toward Applications," *Science*, Vol. 297, 2002, pp. 787 – 792.

Figure 1.1 *- Top is a representative graphine sheet showing a wide range of different (m,n) values including the zigzag, m=o and armchair, m=n. A, B, and C, are representative models of single walled carbon nanotubes having different chairalities. D is a scanning-tunneling micrograph of a chiral single-wall carbon nanotube. E is a transmission electron micrograph of a multi-walled nanotube.*

Carbon nanotubes have received a great deal of attention since their discovery because of their unusual dimensions, electron transport properties and strength. All theoretical and experimental results indicate that nanotubes are incredibly strong. Typical measurements indicate a Young's modulus of 1.0-1.3 GPa for multiwall tubes and 1.36-1.76 TPa nm/d for single walled tubes, where d is the diameter of the nanotube in nm [2]. They are also very resilient and are able to accommodate large deformations without irreversible atomic rearrangements of the crystalline structure.

There are several ways of growing various types of nanotubes including laser ablation, arc-discharge, chemical vapor deposition, and gas phase catalytic growth methods. The nanotubes used in the current research were produced by Carbon Nanotechnologies, Inc. [3] using the high pressure CO disproportionation (HiPCO) process [4,5]. This process injects $Fe(CO)_5$ into a stream of CO gas at high temperatures and pressure. The Fe forms metal clusters which act as catalyst sites promoting the Boudard reaction:

$$CO + CO \rightarrow C(s) + CO_2(g)$$

It is believed that when the metal particles achieve a size near that of C_{60} they nucleate and grow SWCNTs. This occurs because a SWCNT is a more stable form of carbon than a spherical carbon coating of a metal cluster when diameters approach 1nm. Nanotubes will continue to grow until the metal cluster, which is also growing with the addition of residual free Fe atoms, reaches a size that favors the formation of a carbon shell around the cluster, ending the CNT growth and producing tubes with average diameters of 1.1nm[4].

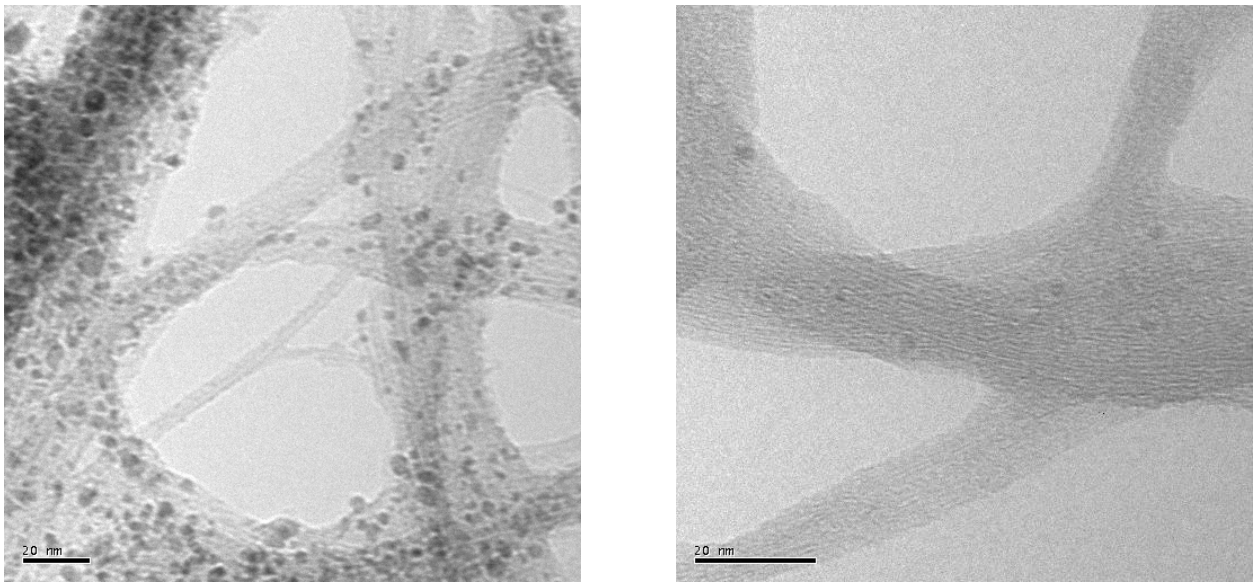

Figure 1.2 *- TEM micrograph of as-produced SWCNT. The dark spots are the Fe catalyst particles or impurities left over from the HiPCO growth process. These CNTs can be purified to greatly reduce impurities as shown in the image on the right [6].*

The HiPco method, while being able to produce large quantities of CNT material, yields a product whose quality has been under question. The nanotubes contain large quantities of impurities, consisting mostly of the Fe catalyst, and require an acid treatment purification process to obtain usable nanotubes. The catalyst is easily seen as the small dark spots in the transmission electron micrograph Fig 1.2 above [6].

Some growth methods offer the possibility of growing CNTs directly on devices in predefined locations; these methods are very expensive, laborious, and inefficient. They have, however, produced CNT based devices capable of making strain sensitivity measurements of a single SWNCT [7, 8, 9].

1.2 Review of Previous Research

Several theoretical and experimental studies on the effects of deformation on nanotube conductance have been reported in recent years [7, 8, 9]. Brief experimental schematics of these studies are included in figure 1.3. In each of these studies, nanotubes were grown in place using chemical vapor deposition (CVD) techniques where catalyst materials were deposited on electrical leads. The CNTs then grown from one catalyst site to another. The left two columns of figure 1.3 used CVD grown nanotubes to span a trench that has been etched into the substrate. This then allows for direct manipulation of the suspended nanotube in the vertical direction. Since the nanotube is fixed at either end to conductive leads, electrical measurements can be made while deforming the tube.

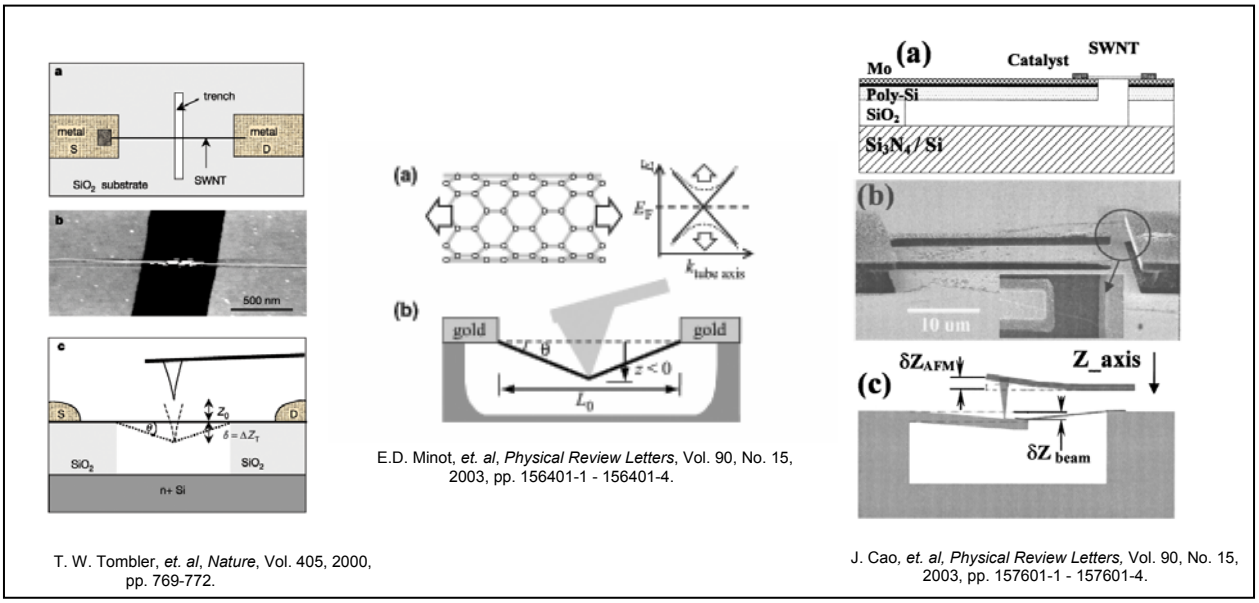

T. W. Tombler, *et. al*, *Nature*, Vol. 405, 2000, pp. 769-772.

E.D. Minot, *et. al*, *Physical Review Letters*, Vol. 90, No. 15, 2003, pp. 156401-1 - 156401-4.

J. Cao, *et. al*, *Physical Review Letters*, Vol. 90, No. 15, 2003, pp. 157601-1 - 157601-4.

Figure 1.3 *– A review of other studies similar to work preformed in current thesis. All methods using CVD grown nanotubes. The left two columns show nanotubes suspended over a trench and are deformed vertically by direct manipulation of the CNT. In the third column, a nanotube was suspended from flexible cantilever on one end and fixed at the other.*

The third column in figure 1.3 shows a similar experiment to the first two. However, instead of directly probing the CNT, the nanotube is fixed at one end to a conductive cantilever and the

other end again to a conductive lead. To avoid localized deformations in the CNT caused by direct probing, the cantilever is flexed to elongate the CNT while measuring the conduction vs strain properties. Each of these studies has contributed to the understanding electromechanical strain characteristics in SWCNTs. However, the methods discussed here rely on the production of CNTs by CVD growth methods. The CVD growth of nanotubes tends to be inconsistent and leads to impurities and imperfections in the tube structures. The CVD methods are also costly and produce relatively smaller quantities of CNTs which makes scale-up of production difficult. The advantages to CVD, however, include the possibilities of growing single CNTs precisely where they are needed.

One alternative to CVD tubes is HiPCO tubes which were discussed earlier. These tubes are mass produced in very high quantities, which offers great potential for materials development applications. Other positive qualities include commercial availability, removal of catalyst materials by purification processes, fewer imperfections, and higher consistency from batch to batch. The only trouble is that, they can not be grown in place on a device.

1.3 Purpose

The purpose of this research is to investigate the possibility of using single walled HiPCO carbon nanotubes as strain sensing agents to be used in multi-functional materials systems that are both load bearing and self sensing.

Two SWCNT based devices have been constructed and tested for strain sensitivity. The first embodiment of this system includes a direct straining technique of a CNT bundle using an atomic force microscope (AFM) aided by a virtual reality / haptic force feedback user interface.

Strain sensitivity measurements are accomplished by means of displacing segments of aligned CNT bundles in contact at either end with conductive electrodes. Resistance measurements are made *in situ* while straining takes place.

The second embodiment takes place on a similar CNT based circuit, this time constructed on a flexible polyimide substrate. Straining of the system is done by mounting the flexible substrate containing the CNT device onto an aluminum sheet which is then loaded into a tensile test load frame. Here loading can be modulated while *in situ* resistance measurements are made.

In constructing these samples, bulk nanotubes are suspended in solution and deposited into specific locations using a dielectrophoresis methodology which is later discussed in detail. The potential advantage to this methodology over existing techniques is that nanotubes can be separated into very small ropes or bundles and deposited onto a surface in bulk, making many sensing devices simultaneously in parallel. This allows rapid production and lower cost of such a system. In both configurations described above, the deformation of the single-walled carbon nanotubes should cause an increase in the electrical resistance of the nanotubes. By demonstrating this feasibility, further steps can be taken toward the advancement of future integrated structural health monitoring systems.

1.4 Scope

A theoretical explanation of CNT strain mechanics, dielectrophoresis calculations and predictions for the deposition and alignment of SWCNTs is presented in chapter 2. Here dielectrophoresis calculations including methods for calculating the dielectrophoretic force on both metallic and semiconducting CNTs, as used to align and deposit CNTs, are described in

detail. Applying the theory requires the development of test samples. The CNT device design and fabrication methods are presented in chapter 3 including photo and electron beam lithography as well as experimental data showing detailed imagery of controlled CNT depositions. Testing of the samples by means of the direct displacement of the CNTs first began by simple proof of concept experiments in which CNTs were displaced using the Nanomanipulator® and atomic force microscopes which are discussed in chapter 4. This initial work included the investigation of self-assembled monolayers (SAM) as a means of facilitating CNT manipulation with the Nanomanipulator®. Investigation of SAMs led to the development of a method which consistently produces aligned CNTs between two electrodes in user defined locations. This work is also described in chapter 4.

Deformations are made in single CNT bundles using the Nanomanipulator® in which the CNTs have been deposited onto a thin film circuit constructed on an oxidized silicon wafer. These tests provide evidence for CNT strain sensitivity based upon strong correlation between changes in localized deformation and changes in resistance and are presented in chapter 5. The second embodiment of a strain sensitive device is presented in chapter 6. Here a flexible CNT based circuit was developed using an architecture similar to the samples used in the direct deformation experiments in chapter 5. In this case, samples were mounted to an aluminum test coupon which was subjected to axial loading. Resistance measurements were made and compared to the loading data. Results indicate high resistance sensitivity to loading. A discussion of the results of the data collected in this thesis is then presented in chapter 7 followed by recommendations for future research.

Chapter 2: Theory

2.1 Dielectrophoresis

To build the CNT test specimens, a method is needed to control the deposition and alignment of the CNTs to position them into desired locations. One method which has been demonstrated to be highly effective uses a dielectrophoresis (DEP) electric field alignment method.

Recent literature and NASA research have shown both single walled and multiwalled nanotubes align to the field lines of an externally applied alternating electric field through a process known as dielectrophoresis [10-15]. Dielectrophoresis is the translational motion of neutral matter caused by polarization effects in a nonuniform electric field [16]. This phenomenon rises from the static polarizability of nanotubes. The polarizability of SWCNTs under constant fields parallel to the cylindrical axis is highly dependent on the tube's electronic structure. In contrast, the polarizability for fields perpendicular to the axis only depends on the tube radius. The relative magnitudes of these two quantities suggest that under the application of a randomly oriented electric field, nanotubes acquire dipole moments pointing mainly along their axes, with the size of the dipole inversely proportional to the square of the minimum direct band gap[11]. By taking advantage of the induced dipole, electric fields can be used to align the CNTs. One point of interest is the fact that these findings indicate a dipole dependence on the electronic structure of the CNT. This means the some varieties of CNTs should align better than others and suggests that under the proper conditions, an applied electric field could be used to sort out different species of tubes from one another.

Interestingly, AC fields will only move uncharged particles. Particulate contaminants in the CNT suspensions, such as dirt or dust, are often charged particles. If using a DC alignment method, the contaminants will be aligned and deposited along with the CNTs. The high frequency (in the MHz range) AC field eliminates this problem and only aligns the neutrally charged nanotubes.

Considering a simple case of a dielectrophoretic force acting on a dielectric sphere as shown by Pohl [16] we get the relationship

$$F_{dep} \propto \varepsilon_m \frac{\varepsilon_p - \varepsilon_m}{\varepsilon_p + 2\varepsilon_m} \nabla E^2{}_{RMS} \qquad (1)$$

where ε_p is the dielectric constant of the particle, ε_m is the dielectric constant of the medium and E_{RMS} is the average field strength. In this case ε_p can be broken into two sub categories, semiconducting and metallic. Metallic CNTs are expected to have very high dielectric constants, and have been suggested to have an effectively infinite polarizability [11]. Depending on the sign of

$$\varepsilon_m \frac{\varepsilon_p - \varepsilon_m}{\varepsilon_p + 2\varepsilon_m} \qquad (2)$$

from equation *(1)* above, the force acting on the CNT is either positive, attracting the CNT to the higher field density, or negative, repelling it. For this particular work the CNTs were dispersed in toluene having a dielectric constant of 2. From Krupke, et al. [14] we find that $\varepsilon_p < 5$ for semiconducting CNTs. Equation *(1)* then implies that for semiconducting CNTs where $2 < \varepsilon_p < 5$ the CNTs will have a positive dielectrophoretic force and will be attracted to the higher field gradients, thus aligning the CNTs. If $\varepsilon_p < 2$, they will be repelled from the field gradients. For metallic CNTs $\varepsilon_p >> \varepsilon_m$ so that F_{dep} is always positive.

For semiconducting CNTs, static polarizability calculations were made by Benedict et al. [11] for 16 different CNT species. These calculations are included below and have been supplemented with additional force calculations which use the static polarizability in the axial direction, α_{zz}, the CNT's length l, and the particular DEP alignment case described in this thesis. Pohl [16] relates force to polarizability as follows: the dielectrophoretic force acting on a dipole in a nonuniform electric field is equal to the length of the dipole multiplied by its polarizability, local field, and the field gradient. Then

$$F_{DEP} = l(\alpha_{zz}\varepsilon_o)(E_e \cdot \nabla)E_e \qquad (3)$$

thus

$$F_{DEP} = \frac{l}{2}(\alpha_{zz}\varepsilon_o)\nabla|E_e|^2 \qquad (4)$$

For simplicity, the average length of the nanotubes is assumed to be *300nm*. This length is consistent with atomic force microscopy measurements made on deposited nanotubes after approximately 24 hours in a bath sonicator and is used for all subsequent calculations. Due to the complex geometry of the applied field, the gradient was determined using a finite element model shown below in figure 2.1. Here a 10V potential was placed on the electrode and a 0V potential boundary on the axis of symmetry between the tips. This geometry is illustrated in figure 2.1 and 2.2 but is discussed in further detail later in chapter 3. The finite element software solves Maxwell's equations over a self refining mesh. From these results, the electric field and the gradient of the electric field can be plotted and are shown in figure 2.1.

The force is calculated along six different lines on the surface between the two tips, each time at different distances from the electrode tip as shown later in figure 2.2. Five lines are

perpendicular to the tip and one is parallel with it and is positioned directly between the two electrodes.

The force calculations for the metallic CNTs require a different approach. In the semiconductor case, force calculations are made using the polarizabilities of the nanotubes given by Benedict *et al.* [11].

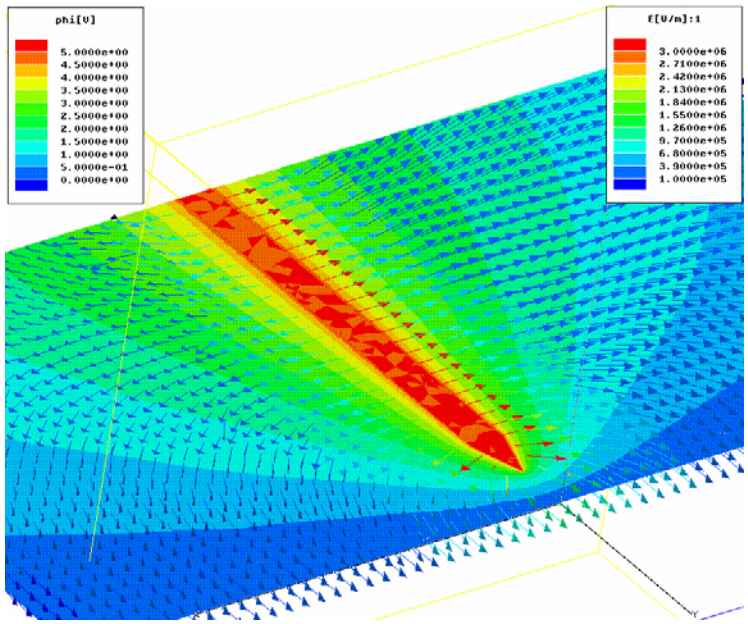

Figure 2.1 *- Finite element prediction of the applied field gradients in region near the alignment electrodes.*

For metallic tubes with chiral vectors where n-m is a multiple of three, having zero band gap, they claim the nanotubes have an effectively infinite polarizability so that equation *(4)* no longer applies. The polarizability, however, is not truly infinite. Thus a different approach is required to determine the force exerted on the CNTs under DEP.

It is known from classical physics that a conductive material in the presence of an electric field will redistribute electrons on its surface such that there is no electric field inside the material. In other words, the material polarizes itself in response to the applied field to keep its internal field zero. This also applies to conductive nanotubes, but only to a point. Since carbon

nanotubes are so small, the actual number of atoms and the related number of mobile electrons becomes very significant. If the applied electric field becomes high enough, it could be possible that there are not enough valence electrons in the nanotube to cancel the applied field in the interior of the tube. In this case the polarizability is, in fact, not infinite.

To calculate the number of electrons needed to keep the internal field zero for this experimental case, an applied field of 10Volts / 3microns is used. This is the field strength used experimentally in the current research. Then from [17] the following equation

$$E_{ext} = \frac{q}{4\pi\varepsilon_o r^2} \qquad (5)$$

where E_{ext} is the external applied field and ε_o is $8.85 \times 10^{-12}\ C^2/(N*m^2)$, the total charge q in coulombs needed to oppose the applied field can be calculated. Dividing q by the charge per electron, $e = 1.602 \times 10^{-19}$ *coulombs,* results in the number of electrons needed to oppose the applied field. For this experimental case with an applied field of *10Volts / 3mircons* and an assumed nanotube length of *300nm* (*r=150nm*) there are approximately 52 electrons needed to zero the internal field.

Equation *(5)* is used to determine how many electrons are needed, but, as mentioned before, this does not necessarily mean there are that many available. To determine the number of electrons available an additional calculation is needed based upon condensed matter physics.

Using this approach requires some background into solid state and condensed matter physics. There are three particular concepts which will be used to determine the number of electrons available in the nanotubes to oppose the electric field: the Fermi energy, the Fermi function, and the density of states.

At absolute zero, electrons arrange themselves into the lowest possible energy state. Since electrons are fermions having half-integral spin, they must obey the Pauli exclusion principle, which states that electrons are not able to occupy identical energy states. The Fermi energy level then is the energy level below which all of the electrons sit idly in the lowest available energy states and infinitesimally above which empty higher energy states are available for activated electrons.

The Fermi function *f(E)* gives the probability that a given available electron energy state will be occupied at a given temperature. The Fermi function comes from Fermi-Dirac statistics [18] and has the form

$$f(E) = \frac{1}{e^{(E-\varepsilon_f)/kT} + 1} \qquad (6)$$

Where ε_f is the Fermi level, k is Boltzmans constant = $8.617 \times 10^{-5}\ eV\ K^{-1}$, and T is temperature in Kelvin. The Fermi function gives the probability of occupying an available energy state, but this must be multiplied by the number of available energy states at the Fermi energy to determine how many electrons would reach the conduction band. This density of energy states is called the electron density of states or just density of states. Saito, et al, [1] state that for all metallic nanotubes, independent of their diameter and chirality, the density of states at the Fermi energy per unit length along the nanotube axis is a constant given by

$$N(E_F) = \frac{8}{\sqrt{3}\pi\alpha|t|} \qquad (7)$$

where $\alpha = 2.49$ *Å* is the graphine lattice constant, and $|t| = 2.9$eV is the nearest-neighbor carbon-carbon tight binding overlap energy. Multiplying the Fermi function by the density of states at the Fermi energy and integrating from the Fermi energy to infinity results in the number electrons above the Fermi level per unit length of the CNT:

$$Number(E) = \int_{\varepsilon_f}^{\infty} \frac{N}{e^{(E-\varepsilon_f)/kT} + 1} dE \qquad (8)$$

Here N is the density of states from equation *(6),* ε_f can be set to zero, *k* is Boltzman's constant, $k = 8.617 \times 10^{-5}\ eV\ K^{-1}$, and T is temperature in °*K*. The average length of a nanotube is assumed to be *300nm* and a temperature of *295°K* is used for the calculations. This results in *10* electrons available in the conduction band of the nanotube.

A final correction must be considered as change in potential energy, *Δu, which* is the average energy gained by an electron moving from one end of the tube to another due to the applied electric field:

$$\Delta u = qEl \qquad (9)$$

The electrons near the Fermi energy level can exchange electrostatic potential energy for chemical energy and move above the Fermi surface where they are free to move along the tube. The net effect is a downward shift in the Fermi surface by the electrostatic potential energy gain of the electrons in moving down the tube. While the assumed average tube length is 300nm, the average electron moves half the length of the CNT. Thus for equation *(9), l=150nm*. The

applied field is 10Volts / 3mircons and the charge of an electron is 1eV, Δu is then equal to approximately *½ eV*. In terms of equation *(8),* this yields:

$$Number(E) = \int_{-\Delta u}^{\infty} \frac{N}{e^{(E-\varepsilon_f)/kT}+1} dE = \int_{-1/2}^{\infty} \frac{N}{e^{(E-\varepsilon_f)/kT}+1} dE \qquad (10)$$

Equation *(10)* produces a total of 305 electrons above the Fermi surface. In this case there are enough electrons available to oppose the applied electric field. However at some higher field strength, when the number of electrons available is less than the number needed to oppose the electric field, this may no longer be true if $\Delta u = qEl$ is not too large.

Using these calculations, dielectrophoretic force approximations for metallic SWCNTs can be made using a classic dipole moment calculation in which two charges q are separated by a fixed distance s in the presence of a nonuniform field E_{ext}. The dipole moment p is then defined as qs where s is the length of the nanotubes, $s=300nm$, and q is the charge from the 52 electrons calculated in equation *(5):*

$$F_{DEP} = p\nabla E_{ext} \qquad (11)$$

Using equation *(4)* for the semiconducting CNTs and equation *(11)* for the metallic CNTs (and small band gap semiconductors), dielectrophoretic forces were calculated for a set of different nanotube chairalities along the 6 different lines illustrated in figure 2.2. These are plotted below in figures 2.3 and 2.4 and The maximum DEP forces at each location are displayed in table 2.1.

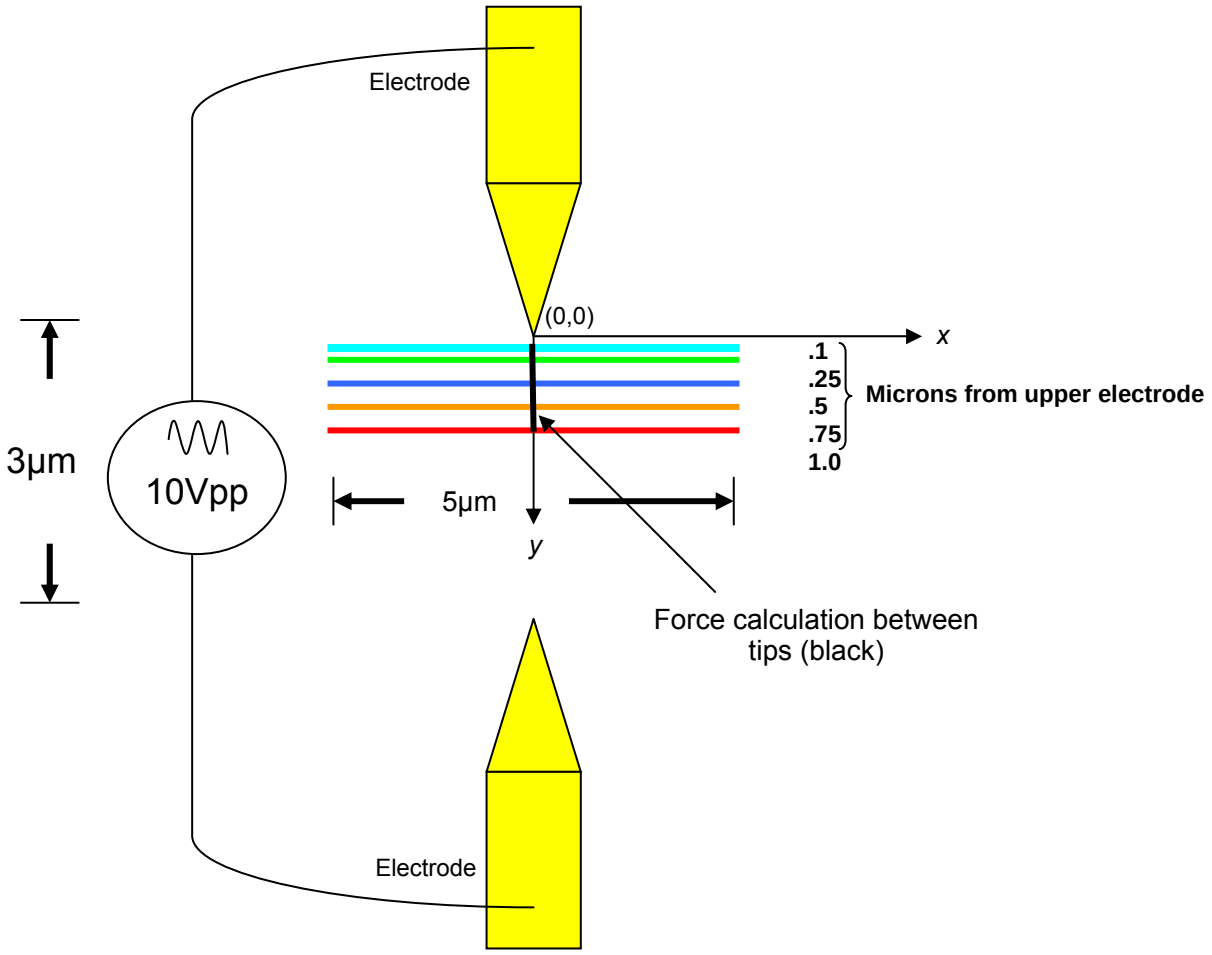

Figure 2.2 *- Schematic of experimental geometry and locations of dielectrophoresis force calculations.*

Table 2.1 is a composition of (n,m) values with corresponding CNT radii, and their calculated polarizability from reference [11]. Note that small band gap semiconductors (chiral vector (3q,0) for int q) were treated as metallic CNTs for polarizability calculations. This data is supplemented with the DEP forces per unit length (N/Å) calculated for the specific geometry of this experiment.

Tube (n_1,n_2)	R	α_{zz}	F_{max} (.1μm)/Å	F_{max} (.25μm)/Å	F_{max} (.5μm)/Å	F_{max} (.75μm)/Å	F_{max} (1μm)/Å
*(9,0)**	3.57		4.34E-14	9.19E-15	1.92E-15	8.34E-16	4.25E-16
(10,0)	3.94	174.7	4.84E-19	5.15E-20	6.02E-21	1.95E-21	8.75E-22
(11,0)	4.33	171.6	4.76E-19	5.06E-20	5.91E-21	1.92E-21	8.59E-22
*(12,0)**	4.73		4.34E-14	9.19E-15	1.92E-15	8.34E-16	4.25E-16
(13,0)	5.12	292.4	8.11E-19	8.62E-20	1.01E-19	3.27E-21	1.46E-21
(14,0)	5.52	268.3	7.43E-19	9.24E-21	9.24E-21	3.00E-21	1.34E-21
*(15,0)**	5.91		4.34E-14	9.19E-15	1.92E-15	8.34E-16	4.25E-16
(16,0)	6.30	445.5	1.24E-18	1.31E-19	1.53E-20	4.97E-21	2.23E-21
(17,0)	6.70	401.4	1.11E-18	1.18E-19	1.38E-20	4.49E-21	2.01E-21
*(18,0)**	7.09		4.34E-14	9.19E-15	1.92E-15	8.34E-16	4.25E-16
(19,0)	7.49	651.1	1.81E-18	1.19E-19	2.24E-20	7.28E-21	3.26E-21
(4,4)	2.73		4.34E-14	9.19E-15	1.92E-15	8.34E-16	4.25E-16
(5,5)	3.41		4.34E-14	9.19E-15	1.92E-15	8.34E-16	4.25E-16
(6,6)	4.10		4.34E-14	9.19E-15	1.92E-15	8.34E-16	4.25E-16
(4,2)	2.09	49.1	1.36E-19	1.45E-20	1.69E-21	5.49E-22	2.45E-22
(5,2)	2.46		4.34E-14	9.19E-15	1.92E-15	8.34E-16	4.25E-16

Table 2.1 *- Table of maximum dielectrophoretic forces along lines at set distances from the electrode tips. The first three columns are taken from reference [11]. The polarizabilities, (α_{zz}), were used to calculate the dielectrophoretic force on the semiconducting SWCNTs when a 10V difference is applied between electrodes 3μm apart. Metallic CNTs are shown in blue. The * indicates small-gap semiconductors.*

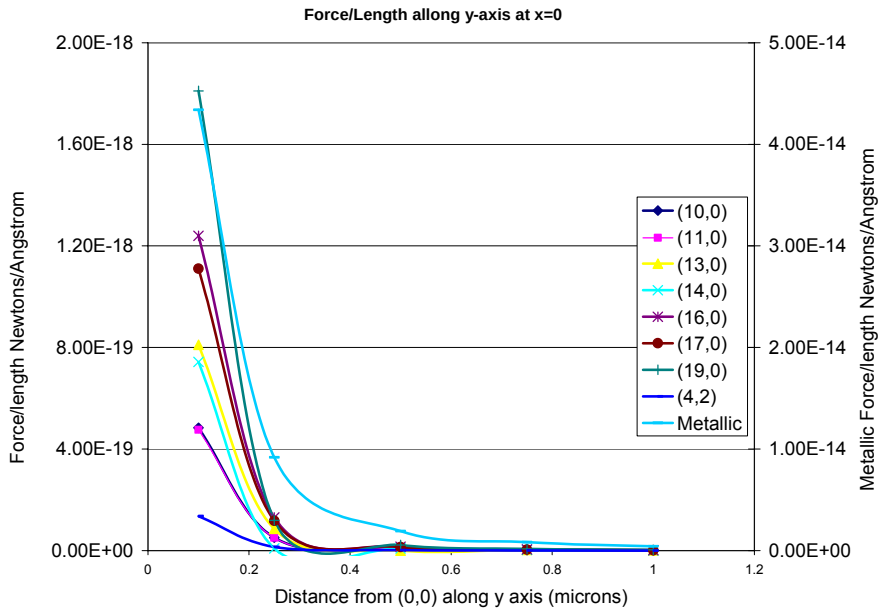

Figure 2.3 *- This plot shows the maximum DEP force/length nanotubes between the two electrodes shown in figure 2.2 above.*

These findings indicate that there is substantially more DEP force on the metallic nanotubes than on the semiconducting tubes, about four orders of magnitude more. Additionally the metallic peaks are broader, which allows for greater attractive forces at larger distances from the electrode tips.

To understand how this force translates into nanotube alignment it is necessary to condsider how the nanotubes behave in solution. Nanotubes undergo what is known as Brownian motion, which is simply the random movement of microscopic particles suspended in a fluid. This motion has an energy of k_bT equal to 2.3×10^{-2}eV or 3.685×10^{-21} Joules. In order for the applied field to have an alignment effect on the nanotubes, the alignment energy must be many times larger than k_bT [19]. Applying this idea to the calculations above, the energy gained in moving a 300nm metallic tube 100nm starting from 1 micron away from the electrode tip is

approximately equal to 32 k_bT. This is more than sufficient to overcome the Brownian motion and align the nanotubes.

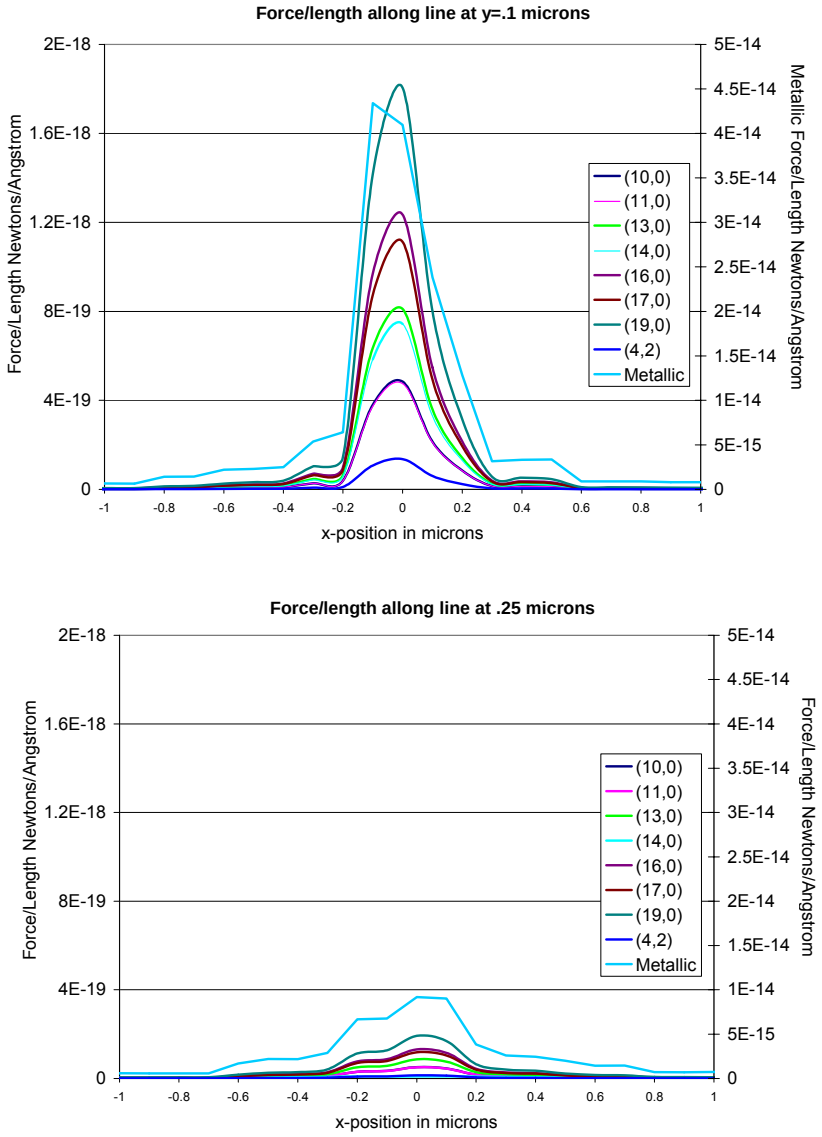

Figure 2.4 *– These two plots represent the DEP forces per unit length of each of the different SWCNT types along the two closest lines to the electrode tips, .1μm and .25μm.*

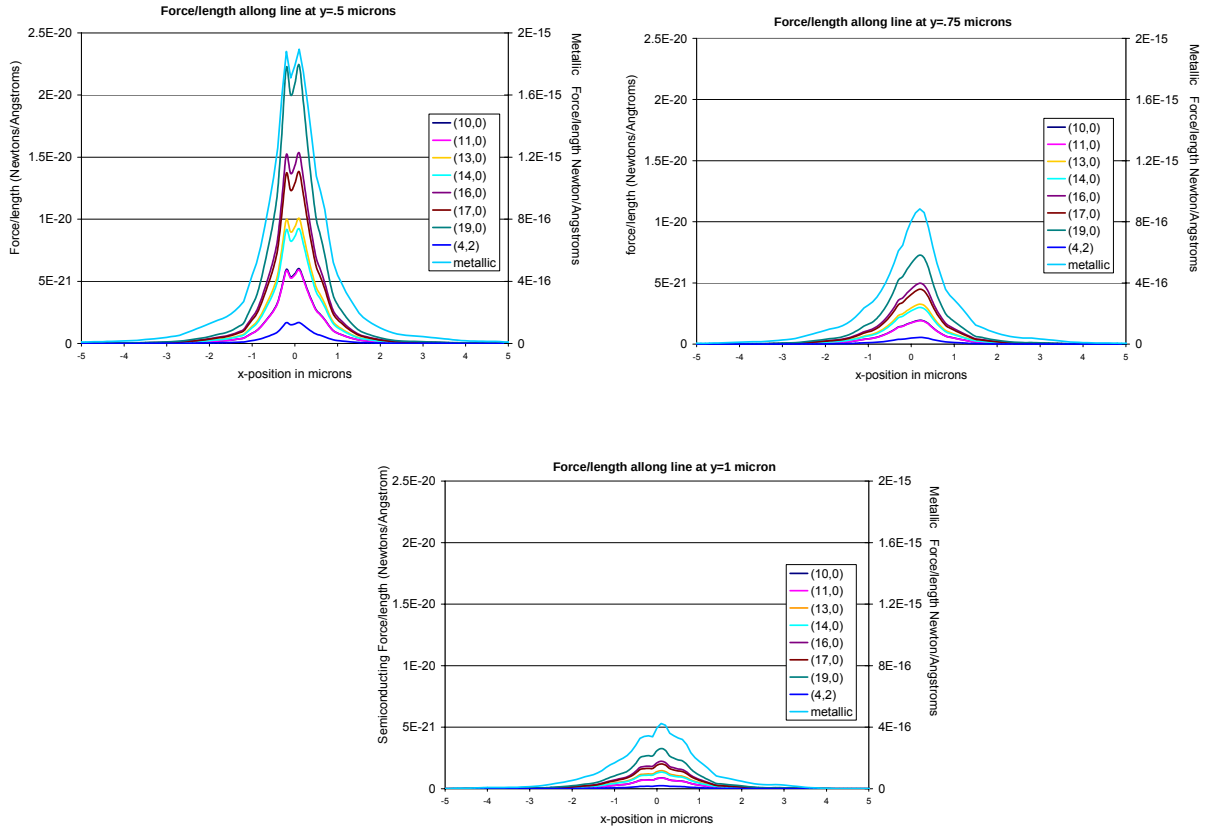

Figure 2.4 continued *- These plots represent the DEP forces per unit length of each of the different SWCNT types along the remaining three lines; .5μm, .75μm and 1μm shown clockwise.*

In the case of the semiconducting tubes, the energy gained in the tubes is always less than k_bT for all of the cases studied here, reaching approximately $.1\ k_bT$ for the (19,0) case at .1μm from the electrode. Figure 2.3 shows the peak DEP forces between the two electrodes and indicates that the DEP forces grow exponentially with proximity to the electrode tip. From this it is possible to infer that at some distance very close to the tip, the DEP forces will be great enough to overcome the Brownian motion and align with the field lines.

The data presented here suggest that dielectrophoresis has a very good potential to sort nanotubes, pulling out both the metallic nanotubes and small band gap semiconducting CNTs from the solution and depositing onto the sample surface. The DEP force can draw these

nanotubes in from over one micron away from the electrode tip and align them to the field lines between the electrodes.

2.2 CNT Strain Mechanics

In 1997, a report published by a group of French scientists [20] predicted that uniaxial stress applied parallel to the axis of the carbon nanotubes can significantly modify the nanotube's band gap. For zigzag tubes, with chiral vector *(n,0),* they showed that this behavior is strongly dependent on whether *n=3q, 3q-1, or 3q+1 where q is an integer.* The theoretical simulation of the band gap vs. stress showed that the band gap changes linearly with stress for zigzag tubes whereas armchair (metallic) nanotubes, with chiral vector *(n,n),* remained metallic through all strains in the study. In particular, semimetallic CNTs, which are a subset of zigzags tubes having a chiral vector *(3q,0)* for *int q,* are predicted to be the most sensitive.

Recently several experimental reports have confirmed the theoretical model described above using individual, grown-in-place SWCNTs. In terms of the physical properties of the nanotubes, there should not be any difference between straining a grown in place CNT or a deposited HiPCO CNT. However, HiPCO CNTs are very difficult to exfoliate into single tubes and are found most often in bundles ranging in size from 4nm up to approximately 30nm in diameter. Because of the CNT bundling, it is difficult to pinpoint the exact nature of any expected resistance change. There are two distinct phenomena that could cause this behavior. First is the already known and understood straining of the individual CNTs themselves, where in fact the conduction band gaps are modulated by induced strain as cited above. Second is the possibility for tube-tube interaction. In the bundles, the CNTs are not anchored and have the

ability to slide across one another with relative ease. This could cause a possible change in the conductance of the CNT bundle.

A CNT sample was fabricated using the dielectrophoretic CNT deposition methods and device fabrication methods described later in this thesis. The sample was then used for conductivity testing and was subjected to cryogenic temperatures in a SQUID magnetometer down to 5°K. Every 20°K an I-V curve was taken to observe any effects of temperature on conductance.

The SQUID Magnetometer is a specialzed piece of testing equipment designed for low temperature studies as and/or magnetic material properties and characterization. The system consists of a liquid helium cooled sample section in which sample temperatures can be taken slightly below 5°K. In addition, the magnetometer is equipped with a Superconducting magnet capable of applying up to a 7 Tesla magnetic field at the sample location.

The data are shown below in figure 2.5. Here one can observe the transition from the linear metallic behavior at room temperature to the semiconducting behavior at very low temperatures consistent with a small band gap nanotube. The data shown are very similar to those obtained in a similar test reported in reference [21], and shown at the bottom of figure 2.5.

Since the theoretical work of reference [20] predicted no change in the band gap of the metallic CNTs, it was important to demonstrate that the CNT bundles in the present work show semiconducting behavior making these bundles strain sensitive. The data in figure 2.5 confirm just that.

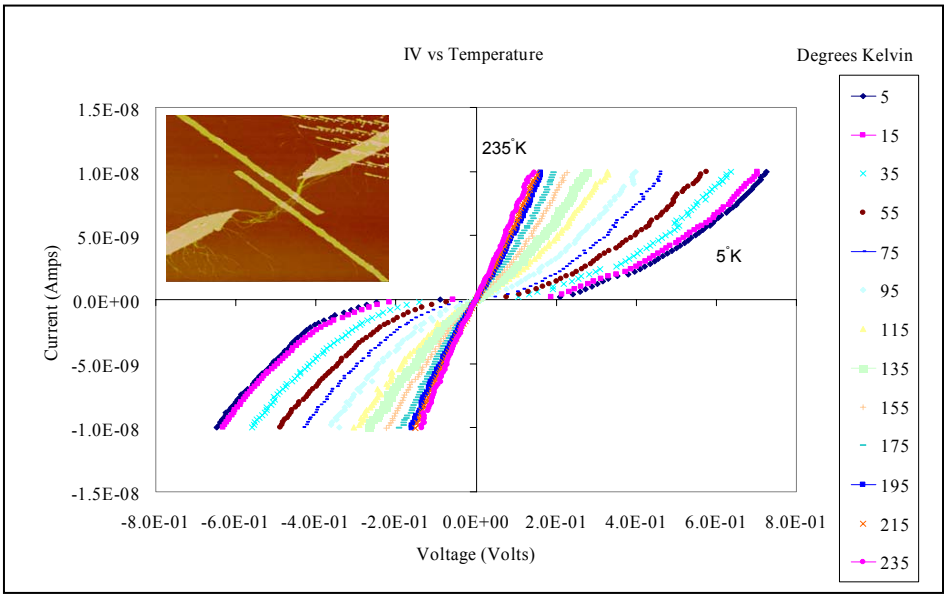

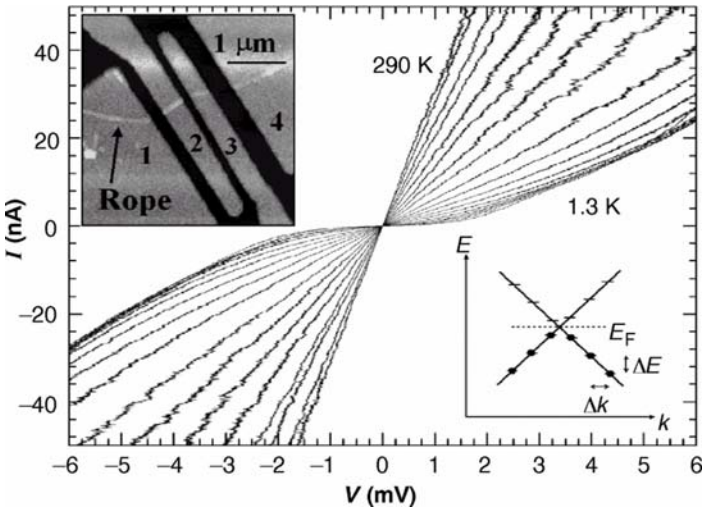

Figure 2.5 *- I-V measurements taken of CNT ropes at different temperatures from 5°K to 235°K shown at top. Below are similar data from reference [21]. Here both data sets illustrate the semi conductive behavior of SWCNT ropes at low temperature.*

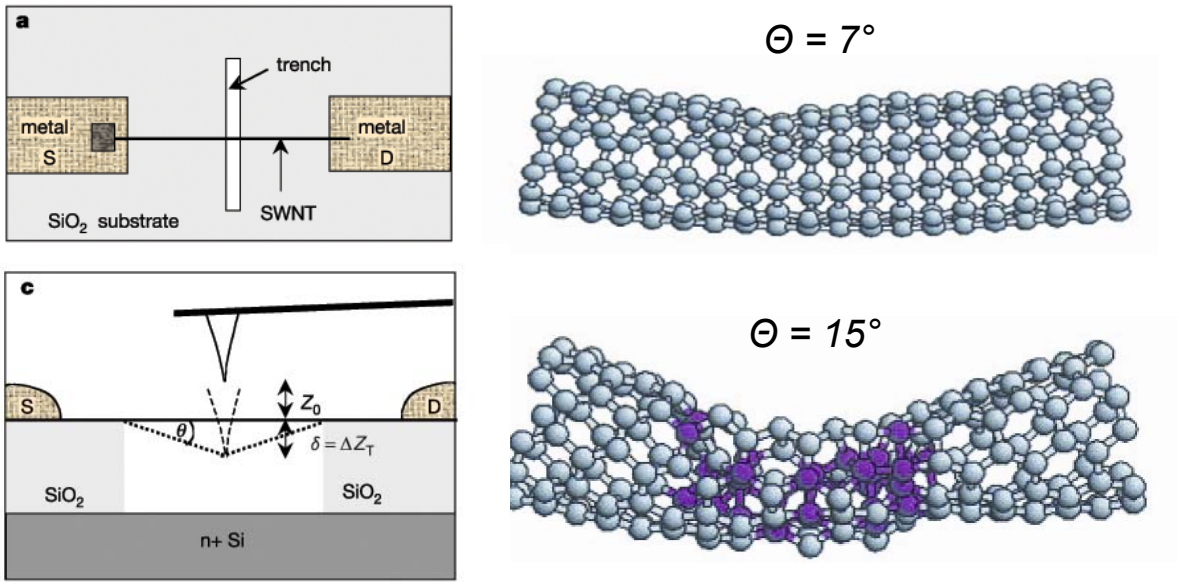

Tombler et al. Nature, Vol 405, 2000

Figure 2.6 - Experiment (left) and theoretical model (right) by Tombler et al. [9]. In this work the AFM tip is used to deform a suspended SWCNT shown in thetop left and bottom left drawings. The AFM tip is displaced vertically while conductive measurements of the device are made. The right two nanotube models illustrate how the AFM distorts the shape of the nanotube.

Experimental data and molecular dynamics modeling of a strained – suspended SWCNT experiment shown in figure 2.6 are given by Tombler et al. [9]. A brief background on carbon – carbon bonds is first needed to fully understand their findings.

In molecular dynamics modeling of carbon it is important to understand the nature of carbon based materials. Carbon, being the sixth element on the periodic table, has six protons and six electrons. The six electrons occupy the $1s^2$, $2s^2$, and $2p^2$ atomic orbitals which in its ground state can more specifically can be written as $1s^2\,2s^2\,2p^2$. The outer orbitals, $2s^2$ and $2p^2$ are known as the valence electrons, which in the crystalline phase can configure themselves into 2s, $2p_x$, $2p_y$, and $2p_z$ orbitals. This arrangement is necessary for covalent bonding and is a key

element in the strength of the carbon nanotubes. In carbon, the energy difference between the 2p and the 2s levels is small compared to $|t|$, the nearest-neighbor carbon-carbon overlap. Therefore the electronic wave functions for the four valence electrons can easily mix with one another in a process called sp^n hybridization, changing occupation of the 2s and 2p atomic orbitals so as to enhance the binding energy of the carbon atom with its neighboring atoms. In doing so, the mechanical wave functions derived from Schrödinger's equation are combined to form an equivalent set of wave functions known as hybrid atomic orbitals. In this case one s orbital combines with three p orbitals to form four equivalent bonds called sp^3 hybridization. Similarly, one s-orbital can combine with two p-orbitals to form 3 equivalent bonds called sp^2 hybridization [1, 22]. Sp^2 hybridization in graphite has a trigonal planer geometry where the hybridized orbitals form σ - bonds between neighboring carbon atoms. σ - bonds are covalent bonds which are very strong having maximum electronic overlap and produce the hexagonal arrangement of the carbon atoms in a graphite sheet. One of the 2p orbitals in each atom overlaps with those of its neighbors to form the π - bonding system where the electrons are delocalized and are free to move about. π - bonds are much weaker than σ - bonds and are responsible for electrical conduction. Diamond for instance, is composed of carbon where the bonds are sp^3 hybridized. In this configuration, all of the bonds are σ - bonds, which explains why diamond is so hard and is also a poor electrical conductor.

Under ambient conditions, nanotubes are composed of carbon in sp^2 bonds. In the work of Tombler et al. [9], shown in figure 2.6, it was found that strong local bonding deformation induced by the AFM tip can be responsible for dramatic conductance decrease in CNTs (shown in purple.) For small bending angles, $\theta \leq 7°$ (refer to figure 2.2) the nanotube retains its sp^2 bonding throughout its structure. As the tip pressure increases, deformations in the CNT start to

distort the bond structure. Bonding between atoms proximal to the tip begin to switch from sp^2 to an sp^3 hybridization while the rest of the CNT remain in an sp^2 state. Further local analysis of the bent nanotube in the tip vicinity reveals the onset of an increase in σ-electrons (electrons in σ-bonds) in the highly deformed local region. This is, however accompanied by a significant decrease in the π-electron (electrons in π-bonds) density. The π-electrons, which are mainly responsible for electrical conduction, are delocalized causing a drastic reduction in the π-electron density, which is responsible for the substantial decrease in conductance.

Additional modeling and experimental work have been done to investigate the electromechanical response of nanotubes under uniaxial stress. As mentioned at the beginning of the chapter, predictions by Heyd, Charlier, and McRae [20], show that discrete density of states energy levels and the gaps are very deformation sensitive. Thus uniaxial stress applied parallel to the axis of the carbon nanotubes significantly modifies the nanotube's band gap. The chirality of the tube plays a large role in its electromechanical behavior. Metallic nanotubes remain highly symmetric under loading and have been predicted to be the least sensitive to strain where as small band gap semiconductors have been predicted to show the largest change in their conductivity under loading. This was confirmed experimentally by Cao et al. [8]. The molecular dynamics of the uniaxial loading case are highly complex with few publications offering any analyses of the transport behavior under loading. The theoretical work by Heyd, Charlier, and McRae [20] indicates that some nanotubes decrease their band gaps while others have an increasing band gaps with applied stress depending on their chirality. Experimental works, however, present conductivity results similar to those of the Tombler paper [7, 8, 9].

Chapter 3 Circuit Design, Lithography, and CNT Alignment

3.1 Circuit and Lithography Design

In order to proceed with the electromechanical testing of carbon nanotubes, a test bed is needed to bridge the small size scales of the nanotubes to something more tangible. The test bed developed in this research was designed around the use of a silicon substrate with a thin film circuit deposited on it. A simple circuit has been designed to provide access to conductive measurements of the CNT while leaving a central, current carrying section of the nanotube exposed.

UV lithography can routinely approach features down to about 15-20 micron sized features using commercially available photoplots shown in figure 3.1. In order to have the precision needed for this experiment, a two step lithography process is used to fabricate each sample. It consists of a photolithography step to build all of the larger features followed by an electron beam lithography step which is capable of writing features under 100 nanometers in size, allowing placement of electrodes with nanometer precision. Three different views of the photolithography CAD design are shown in figure 3.1 with the critical dimensions indicated. The left drawing is the complete design for one device. The right two drawings are close-up views of the left drawing used to identify critical design dimensions and to conceptualize the configuration. The electron beam lithography takes place within the 100μm x 100μm area defined by the electrical lead spacing shown in the red box of the bottom right drawing in figure 3.1.

To make solid electrical connections to the device while allowing it to be used in a SQUID magnetometer for magnetic field and temperature dependant measurements, the design is centered on the use of a zero insertion force (ZIF) connector, which has 14 available connections spaced by a .5mm pitch shown in figure 3.2. To use the ZIF connector, the photolithography mask was designed incorporating the .5mm pitch to each of the device's leads.

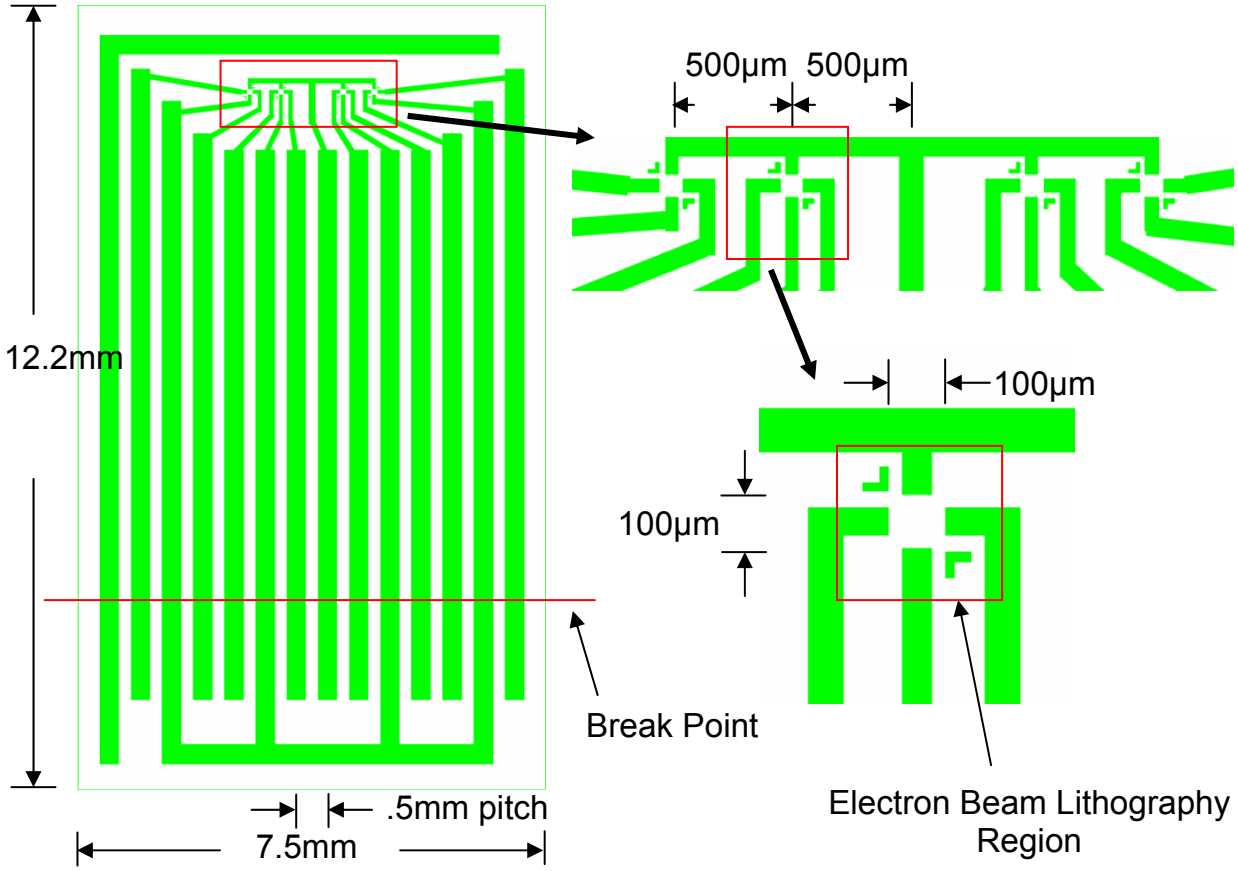

Figure 3.1 *- Photolithography CAD files with close-up views of the main sensor region shown in the right two drawings. Electron beam lithography takes place inside the 100µm x 100µm area defined by the electrical lead spacing shown in the red box of the bottom right drawing. The break point is an arbitrary location at which the sample can be scribed and cleaved to allow for either point probe inspection and alignment techniques or electrical connectivity via the ZIF connector.*

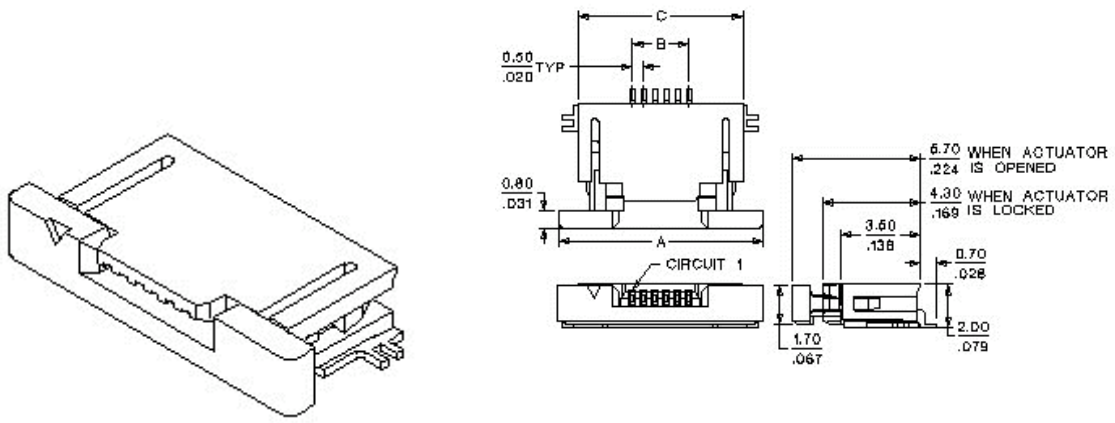

Figure 3.2 *- ZIF Connector chosen for its size and functionality. This particular connector with 14 electrical connections and .5mm pitch will fit inside the SQUID magnetometer and allow for temperature and magnetic field vs. conductivity measurements such as those shown in figure 2.5.*

The L-shaped markings easily identified in the right two drawings in figure 3.1 are the alignment files used by the electron beam lithography to align the e-beam lithography to the photolithography. The lower section of the device has a solid bar which attaches four of the leads. These bottom four leads are used during the CNT alignment process. By connecting them in parallel, a point probe device can also be used to do the alignment process and is able to align all four sensor sections simultaneously. If the ZIF connector is to be used, the device must be cut at the break point pointed out in the left drawing. This is where the device must be scribed and cleaved to remove the lower section such that the four leads are no longer connected in parallel.

The completed photolithography mask is shown in figure 3.3. The design is tiled in an array to cover a large area to make the devices highly parallel. Device spacing was predetermined based on the cutting swath of the dicing saw which is to be used to separate each of the individual devices on a Si wafer.

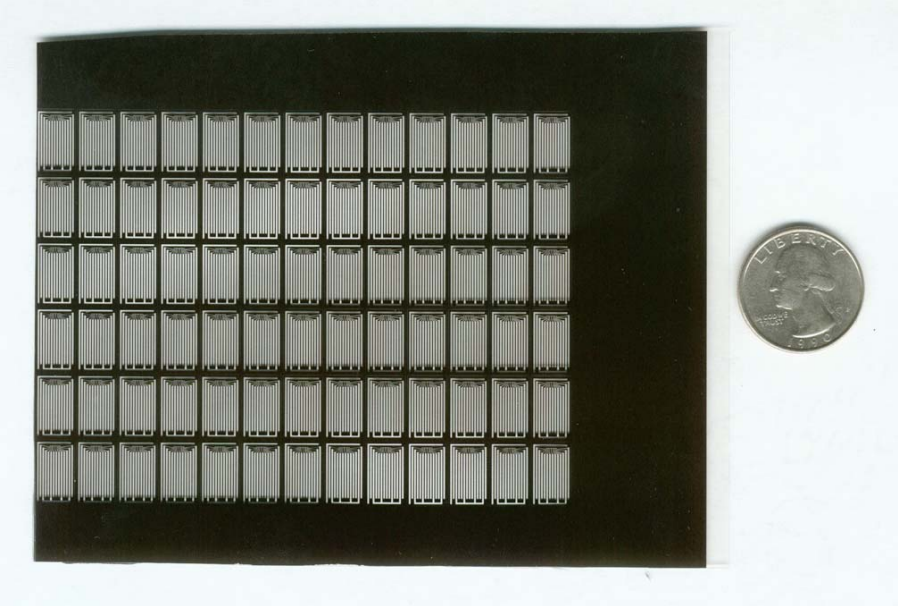

Figure 3.3 *- The final photomask design used for UV photolithography device fabrication. The design is tiled in an array to cover a large area to make the devices in a highly parallel manner. Device spacing was predetermined based on the cutting swath of the dicing saw which is to be used to separate each of the individual devices on a Si wafer.*

The steps in the photolithography process are as follows: Commercially available silicon wafers were used as a substrate with a 500nm oxide thickness. These were cleaned by rinsing first with electronic grade acetone, electronic grade isopropanol, and finally deionized water while spinning in a spin coater at 3000rpm. The wafers were then coated with Shippley 1805 photo resist and prebaked for 30 minutes in an oven at 90 degrees C.

The photomask is placed on the coated wafer on top of which a large piece of quartz covering the entire sample is placed. The quartz is used as a weight to hold the mask securely to the surface of the photo resist and is transparent to the UV light. The sample is then exposed to UV light produced by a mercury arc lamp for approximately 60 sec. Once the necessary exposure is completed the wafer is developed in a solution of Shippley Microposite Developer / de-ionized H_20 mixed 1:1 for approximately 20 sec. The sample is rinsed in De-ionized H_20 and

blown dry with nitrogen. To remove all residues left behind by the protoresist, an oxygen plasma treatment is used for 30 sec. Once completed the sample is ready for metal deposition.

Metals are deposited via electron beam evaporation using the following process. The samples are first coated with a thin adheasion layer consisting of 10nm of titanium or chromium, followed by 30nm of gold to act as the main conducting portion of the circuit. The circuit is made of gold because it is a good conductor, and it does not oxidize. Au does not adhere to silicon well, however, so an adhesion layer of titanium or chromium is needed. The metal is deposited under vacuum of approximately 10^{-6} torr. Upon completion of metallization a liftoff step is required which removes all of the excess metal and resist from the samples. Liftoff is completed by soaking the sample in electronic grade acetone for several minutes followed by ultrasonication in a bath sonicator.

The small relative size of the nanotube and electron-beam circuitry compared to the photolithography allow four individual CNT devices to be constructed on each sample. This design allows all of the devices to undergo CNT alignment and deposition simultaneously in one step by sharing a common top alignment electrode, which allows alignment to take place in parallel without losing access to measurements at each nanotube junction individually.

At this point, each wafer contains several samples which need to be separated for testing and further processing. This is accomplished using a dicing saw in which the sample is first glued to a glass plate using a thermoplastic and then mounted into the saw, aligned and cut. Before the photoplot was laid out, the swath of the saw blade was measured, and this dimension was then used as the lateral spacing of each of the lithography patterns. This ensures that each sample will correctly fit into the ZIF connectors and line up with the contacts. The dicing process requires the sample to be glued to a flat surface using a thermoplastic as the adhesive.

When finished, the excess thermoplastic is needs to be removed and is easily dissolved in acetone, followed by rinsing with IPA, de-ionized water and blown dry with nitrogen.

The sample is now ready for electron beam lithography. The electron beam lithography writes the very smallest features shown in figure 3.4 and is capable of defining features down to about 80nm in size. In this case the lines are 1.5μm wide by almost 50μm long and come to a point at the end.

First the sample is spin coated at 500 rpm for 5 sec. to deposit the electron beam resist, Shippley 920 PMMA A2, 2% in Anisole (Poly methyl methacrylate), evenly over the entire surface. Then the sample is accelerated to 3500 rpm for 30 seconds to produce a thin layer over the sample surface. The sample is placed on a hotplate for 90 seconds at 180°C as a pre-bake step, which evaporates the residual solvent in the PMMA, and then is loaded into the scanning electron microscope.

The electron beam lithography patterns are defined by a user created CAD file. The CAD files is read by the Nanometer Pattern Generation System (NPGS) which is a commercially available upgrade to the SEM. The SEM is set to an acceleration potential of 30kV and a beam current of 20pA. Typically line doses are set to 1.3 nC/cm.

In this case the electron beam lithography design shown in figure 3.4 creates two opposing electrodes at a 3μm spacing which come to a point at the end. Also defined are two alignment "L" shapes which can be used for subsequent electron beam lithography steps, and two squares placed at the interface between the electron beam lithography and the photolithography to maximize the electrical connection between the two.

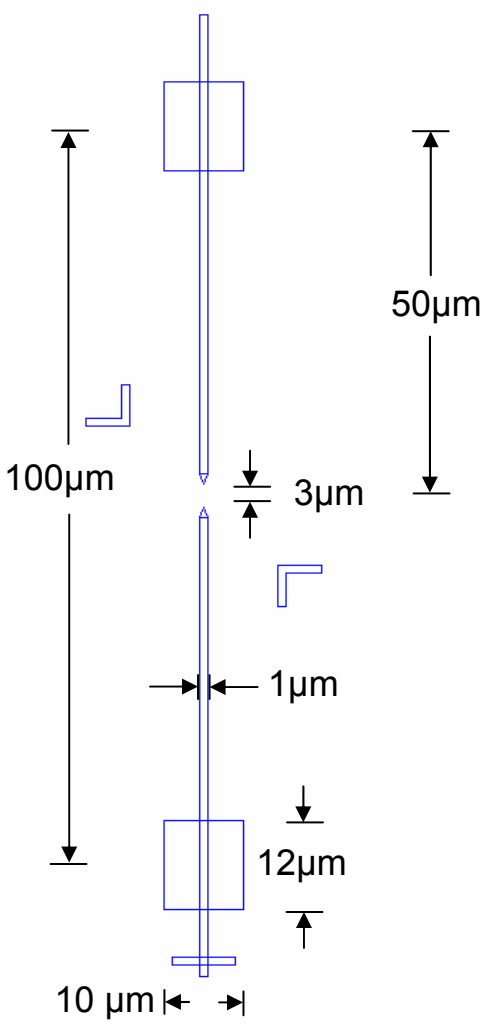

Figure 3.4 *- Electron beam lithography design. The electrode tips come to a point to focus the electric field during alignment and are spaced at 3µm. The squares in the drawing above are placed at the interface between the electron beam lithography and the photolithography to maximize the electrical connection between the two.*

The samples are developed in 3:1 isopropanol (IPA) (electronic grade) and methyl isobutyl ketone (lMIBK) for 70 sec. followed by a rinse in IPA then deionized water and blown dry with nitrogen. The samples are cleaned again using oxygen plasma and are coated with a 10nm Cr adhesion layer followed by 20nm of Au. Liftoff is accomplished by immersion in acetone along with a bath sonication. Samples are then ready for CNT depositions.

3.2 Experimental CNT Alignment

Nanotube deposition was carried out by first dispersing SWCNTs in toluene at a concentration of approximately 1μg/ml and sonicating for 24 hours in a bath sonicator. A sine wave potential of 10Vpp at 5Mhz was applied using a function generator connected to a single end input to differential output circuit, the schematic of which is shown in figure 3.5 (top). This circuit takes the hot lead from the function generator and creates two signals identical to the function generator output but 180° out of phase with each other. A 1MΩ resistor is in parallel with outputs which helps to prevent electrostatic discharge problems to which the nanotubes are very sensitive. Each side of the differential output is connected to opposing electrodes fabricated on the sample surface.

Originally a more simplified circuit was used which put the hot output from the function generator on one electrode which was driven at 10Vpp and grounded the opposing electrode with a 1MΩ resistor in parallel between the electrodes. This produced an uneven distribution of CNTs between the alignment electrodes and resulted in many more nanotubes being collected on the oscillating side.

Interestingly both AC and DC fields have been attempted for CNT deposition. Through the range of frequencies tested, (0-20MHz) there was very little observable difference when looking at the AFM data, however the higher frequencies tended to show only the slightest improvement in alignment characteristics. As mentioned in chapter 2, the AC field will only move uncharged particles. Particulate contaminants in the CNT suspensions, such as dirt or dust, are often charged particles. If using a DC alignment method, the contaminants will be aligned

and deposited along with the CNTs. The high frequency (in the MHz range) AC field eliminates this problem and only aligns the neutrally charged nanotubes.

The separation distances of the electrodes ranged between 3μm and 3.5μm. Several small droplets of nanotube solution are dispensed onto the sample surface by use of a pipette. After a predetermined time, from 15 seconds to 5 minutes depending on the targeted tube density, the nanotube solution is blown off the sample surface with nitrogen.

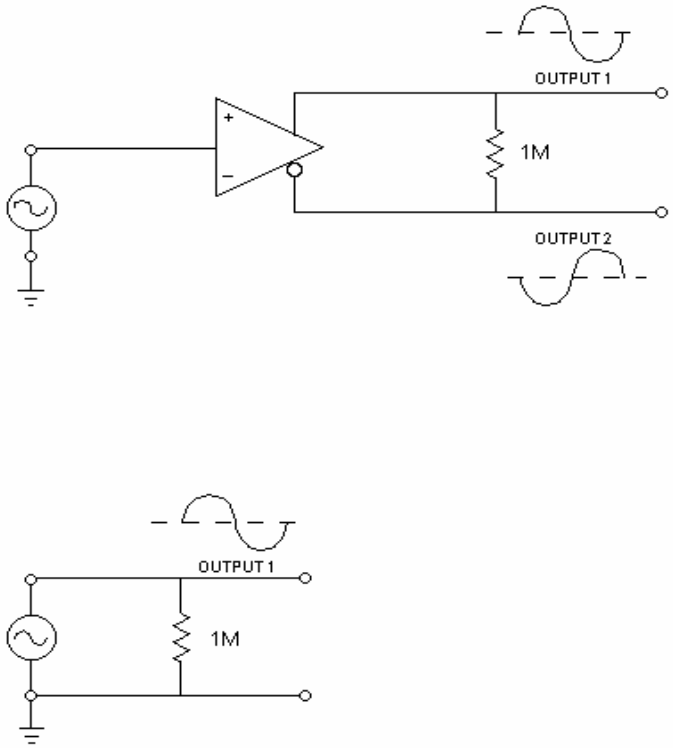

Figure 3.5 *- Single input - differential output circuit show above (top) is used to align the nanotubes. This method drives the alignment signal into the differential circuit which produces two identical outputs 180° out of phase. Below the differential output circuit is another circuit used to align nanotubes. This circuit oscillates the potential of one probe while keeping the other grounded.*

Different tip shapes and configurations of the electrodes have also been used to optimize certain characteristics of the aligned nanotubes. In the current research, the tips of the electrodes come to a point, yielding a highly focused field such that CNTs are aligned in a small region

between the electrodes. To limit the number of CNTs aligned between the electrodes, shorter alignment times are used.

This pointed tip configuration shown in figure 3.4 was modeled with a finite element analysis program to predict the electric fields and electric field gradients. As mentioned in chapter 2 the model places a 10V potential on the electrode and a 0V potential boundary on the axis of symmetry between the tips. The finite element software solves Maxwell's equations on a self refining mesh. From these results, the electric field and the gradient of the electric field can be plotted and are shown in figure 3.6-A. With the understanding that the CNTs will align to the electric field lines as detailed in chapter 2, this model predicts the orientation of deposited nanotubes on a device built and tested under similar conditions. Results shown in figure 3.6-B show such a device built with CNTs deposited as described above for 1 minute. The experimental data show that the CNTs have generally aligned to the predicted field lines. Some entanglement of the CNTs does occur, and therefore not all of the tubes are in perfect alignment.

Other electrode configurations have been tested using two parallel electrodes and a five minute alignment time. This results in a large number of tubes aligned in parallel between the electrodes as shown in figure 3.7. The two images in figure 3.7 were taken on the same sample but in different locations. Both locations were exposed to the same tube solution and for the same time. The left image in 3.7 did not have an applied electric field whereas the right image did. Ideally, the experimental devices would be constructed with only one nanotube between the electrodes to minimize the possible variables in the experiment. This would eliminate the tube-to-tube interaction under loading.

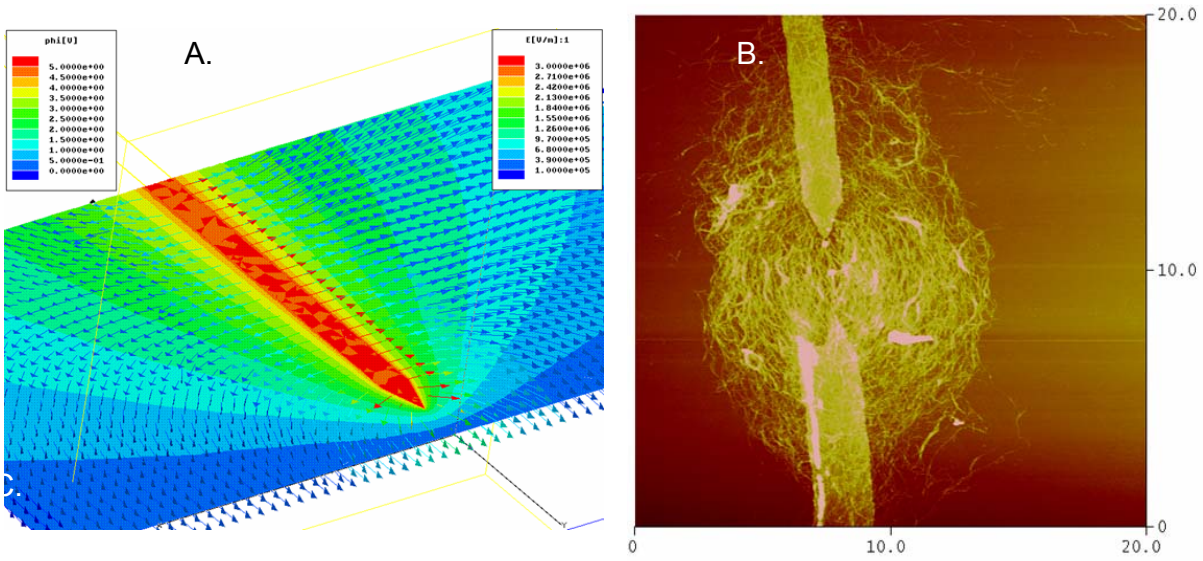

Figure 3.6 *– A - Finite element analysis results showing electric field lines coming from the electrode (in red) and going to a zero-potential boundary simulating the symmetry of opposing and opposite charged electrodes. B – Atomic force micrograph of CNT alignment between two electrodes. The CNTs are aligned to the predicted field lines from the FEM simulation.*

Unfortunately, a single tube device is very difficult to obtain. As mentioned before, the van der Waals forces keep the nanotubes stuck to each other in small bundles. Also, while somewhat controllable, the CNT deposition technique often leaves several to hundreds of CNT ropes deposited and aligned.

Considerable efforts have been made to exfoliate SWCNT ropes. In this work several attempts have been made to create a stable solution of single SWCNTs using different solvents. Ideally the nanotubes would disperse completely into the solution and de-bundle. This however is very difficult to do at the current time.

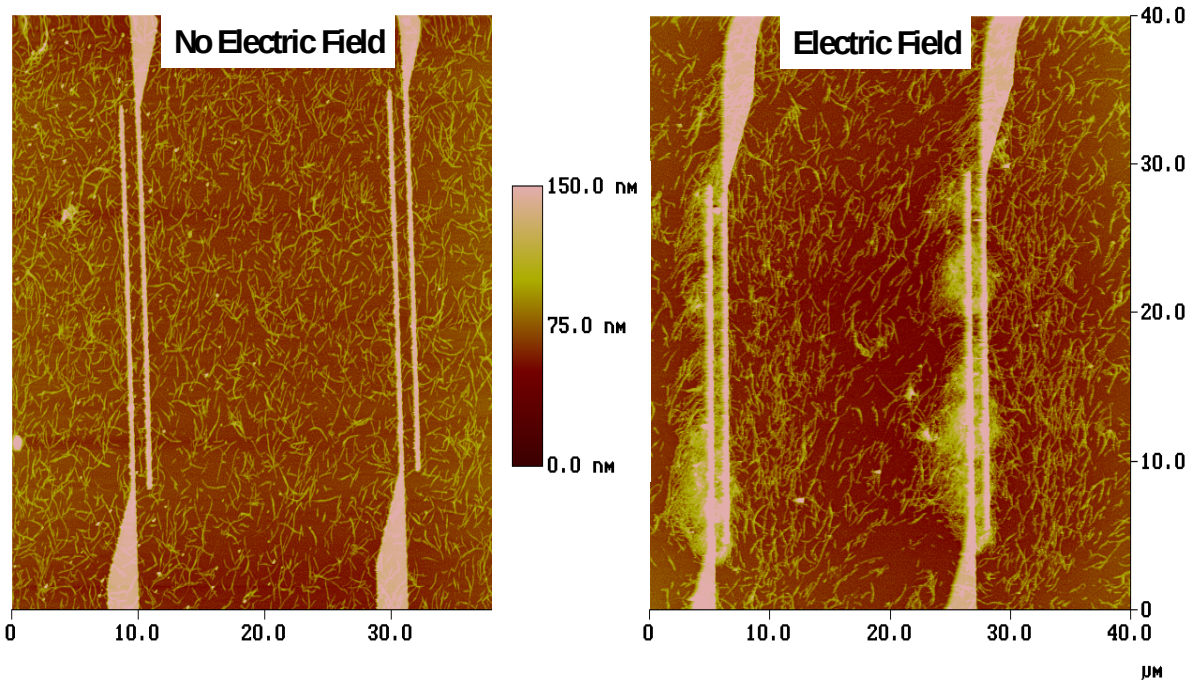

Figure 3.7 *– Comparison between the effect of an applied electric field vs no electric field. Left shows no indication of CNT alignment, the nanotubes appear to have a random orientation. Right shows how the applied electric field draws the CNTs between the electrodes and aligns them to the field lines.*

There have been several reports on this topic by various groups [23, 24, 25] all with a slightly different recipe. However, none has seemed to be able to completely exfoliate single SWCNTs into solution. The method used in the current thesis to produce consistent CNT solutions of small bundles and occasional single tubes disperses the CNTs in toluene at 1μg/ml. This is followed by ultrasonication in a bath sonicator for 24 hours. At this point the CNTs appear to be optically dispersed leaving the solution clear to the unaided eye with no visible suspended particulates. These solutions have proven to be stable for several months at a time. Occasionally the CNTs will precipitate out of suspension, but only 5-10 minutes in the bath sonicator is need to return the solution to an optically dispersed state. This solution was found after trying several combinations of other solvents including acetone, isopropanol, water,

dimethylformamide (DMF), dimethylacetamide (DMA) and different CNT / solvent ratios from very high density to extremely low. Ongoing research at NASA Langley Research Center is aimed at trying to better disperse the CNTs into solution using various techniques including the use of surfactants such as Triton X-100 and Sodium dodecylbenzinesolfonate and other approaches such as functionalization of the CNTs with different chemical groups.

Given that a single tube device is nearly impossible to fabricate at the current time using a CNT suspension, the next best case is to use a single bundle of SWCNTs. Figure 3.8 shows a single CNT bundle that was deposited and aligned between the two alignment electrodes. Further device fabrication put down a second set of electrodes to make a four lead measurement on the bundle. Unfortunately the electrical connections failed before any measurements could be taken; however, height measurements were made using the AFM and are also shown in figure 3.8.

Height measurements were taken using the DI Nanoscope IIIA in tapping mode. CNT diameters are measured from images of CNTs or CNT bundles by measuring the height of the CNT, not the width. This is because the probe used to measure the CNTs comes to a point that is approximately the same size as the CNTs themselves. This introduces error in lateral measurements made on objects which are on the same size scale as the tip radius. Since it is assumed that the CNTs and CNT bundles have circular cross-sections, the height data can be used for accurate measurements of CNT / CNT bundle diameters without introducing errors due to SPM tip width. In the case of figure 3.8 the CNT rope had a diameter of approximately 27nm.

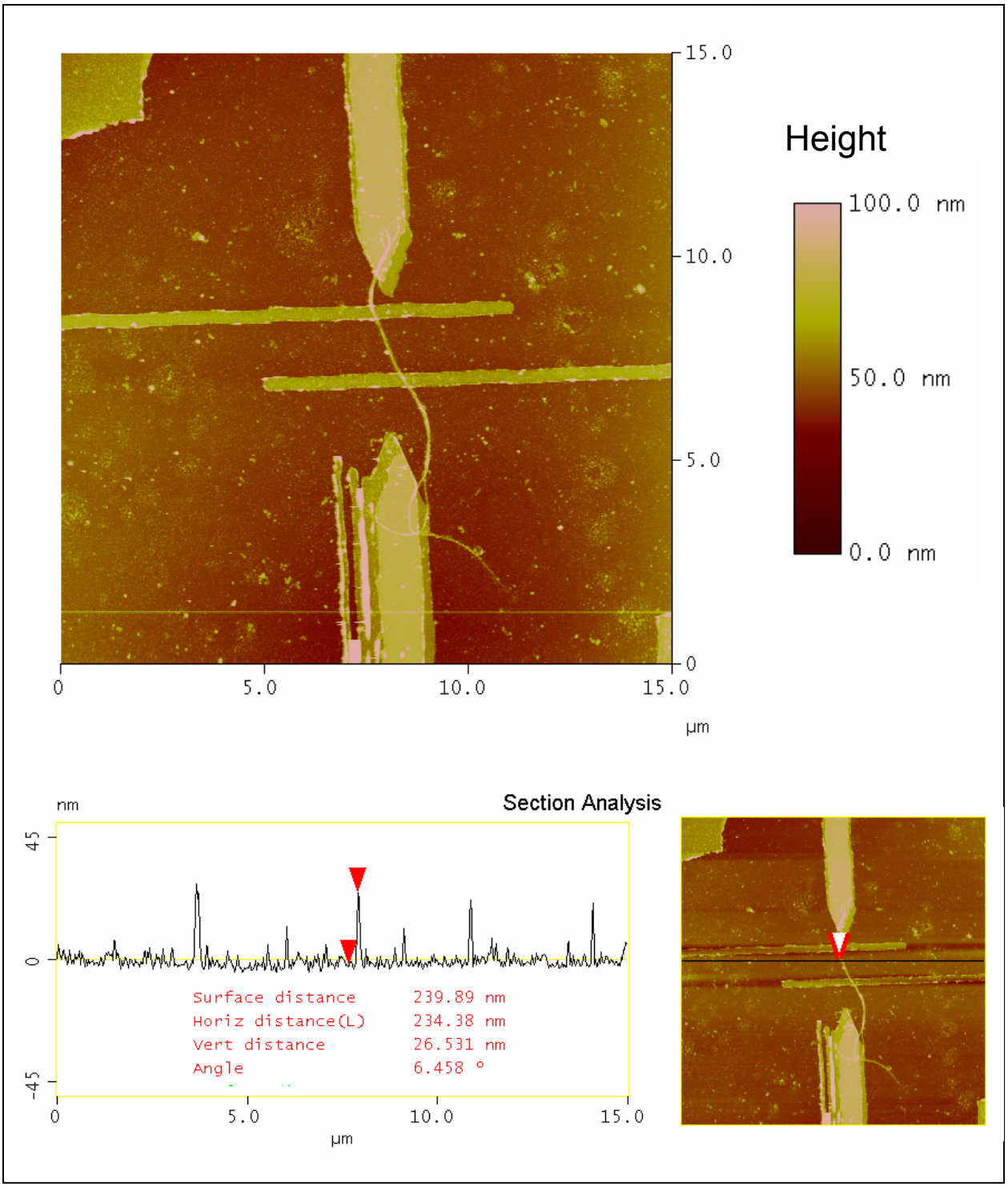

Figure 3.8 *- AFM image of a single CNT rope spanning between two electrodes deposited at 10Vpp at a frequency of 2MHz for 15sec. Right image displays the topography measurement line with measurements shown in bottom right. Data inset bottom left indicates a bundle height of approximately 27nm.*

Chapter 4: Controlled Displacement of Carbon Nanotubes using Atomic Force Microscopy

4.1 Atomic Force Microscopy and the Nanomanipulator®

Scanning probe microscopes and atomic force microscopy have come to the forefront of research instrumentation and have proven their usefulness in materials characterization and analysis. They have led to significant advances in a wide variety of fields including materials science, semiconductor physics, biology, electrochemistry, polymer sciences, tribology, biochemistry, surface thermodynamics, organic chemistry, and nanotechnology, to name a few. Their value as a research tool is due to their unparalleled ability to resolve a variety of interactions between a very small probe tip and the sample surface with atomic resolution. Scanning probe microscopy methods have been designed to measure thermal gradients, magnetic forces, electric forces, van der Waals forces, etc. One of the many benefits of using such a system is that it can be used in ambient conditions, unlike other microscopy methods which usually need to be carried out under high vacuum and risk damaging the sample.

The scanning probe microscope (SPM) used here is the Thermomicroscopes (now Veeco) Explorer coupled with the Nanomanipulator® system shown in figure 4.1. The Explorer uses a fixed sample stage and a flexible cantilever probe on the end of which is a very sharp pyramid shaped tip. The probe is mounted to a set of piezo electric actuators capable of scanning the tip over 100 microns in both the x, and y directions and can move roughly 5 microns in the z direction.

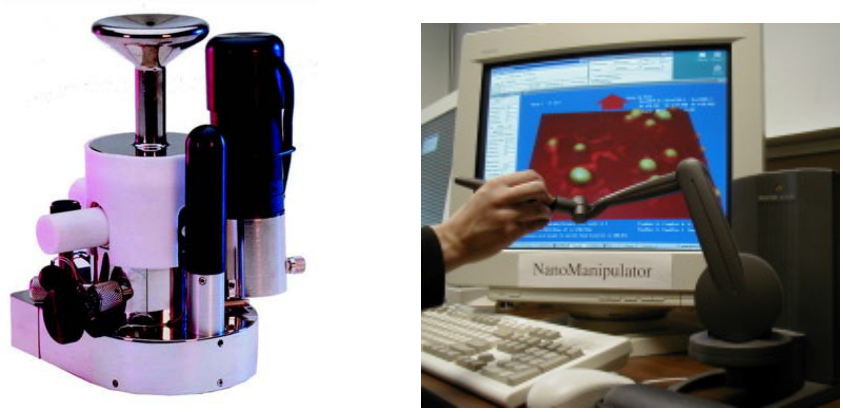

Figure 4.1 *- Explorer atomic force microscope shown left coupled with the Nanomanipulator® user interface shown right is used to make modifications to the surface and manipulate and strain individual nanotubes and bundles with nanometer position control.*

Topography measurements can be made either in contact mode or in tapping mode. In contact mode the tip is moved toward the sample surface while tip deflections are monitored as described below. At approximately 20nm from the surface, interactions between the sample surface and the tip cause the cantilever to deflect. These deflections are measured using a laser which is reflected off the cantilever into a photodetector. In tapping mode, the cantilever is oscillated near its resonance frequency and again brought close to the surface. Tip-surface interactions cause changes in the cantilever's resonance frequency, amplitude and phase. By monitoring these changes, either in tapping mode or contact mode, the system can raster over a user defined area of the sample and map out its topography as shown in figure 4.2.

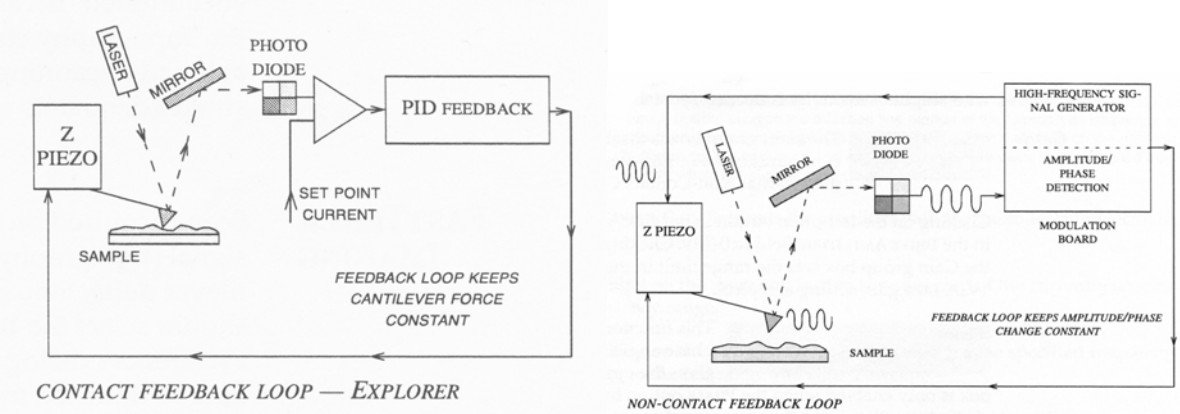

Figure 4.2 *- ThermoMicroscopes –Instrument operation manual schematic of contact mode operation (left) where the AFM tip contacts the surface directly. Tapping mode schematic is shown right with the AFM tip is brought very close to the sample surface where the tip is driven at its resonanve frequency and interact with the vanderwalls surface forces.*

The Nanomanipulator® is a commercially available user interface upgrade to the Explorer AFM. This utilizes a haptic force feed back system and 3D graphics to allow the user to take control of the AFM tip and manipulate submicron sized objects with nanometer precision. This instrument has demonstrated its ability both to displace nanotubes on a sample surface as well as to flex nanotubes in place, repeatedly in a precisely controlled manner, measuring various tip-sample interactions and forces in the process. It is discussed in further detail below.

In this work, the coupling of the Explorer AFM and the Nanomanipulator® has allowed for the imaging and straining of CNTs while conductivity measurements are performed. Imaging the topography of the surface, and modifying the sample, (inducing strain in the CNTs) take place in two different modes of operation; tapping mode and contact mode. The Explorer images in tapping mode and makes its modifications using contact mode. Tapping mode is the preferred method for imaging nanotubes because it provides crisp topological images without disturbing the CNTs through direct contact. As mentioned earlier, in contact mode the tip rasters very close to the surface and can impart translational forces on objects on the sample surface. When the tip

makes contact with the CNTs there is a tendency to bump the CNTs and displace them. This makes contact mode the obvious choice for manipulating CNTs and a poor choice for imaging them, especially when such great care is taken to position them.

Some of the first CNT manipulations for this work, shown in figure 4.3 below, illustrate the feasibility of this methodology. The left two images show before (top) and after (bottom) of a CNT loop which has been pulled by dropping the AFM probe into the center of the loop, and pulling downward [26]. This manipulation was done using the AFM system where the manipulation routine was programmed into the system by the user. The images on the right of 4.3 were done using the Nanomanipulator®. Here the Nanomanipulator® was used to push several bundles of SWCNTs to spell "NASA" as shown in the bottom right image [26].

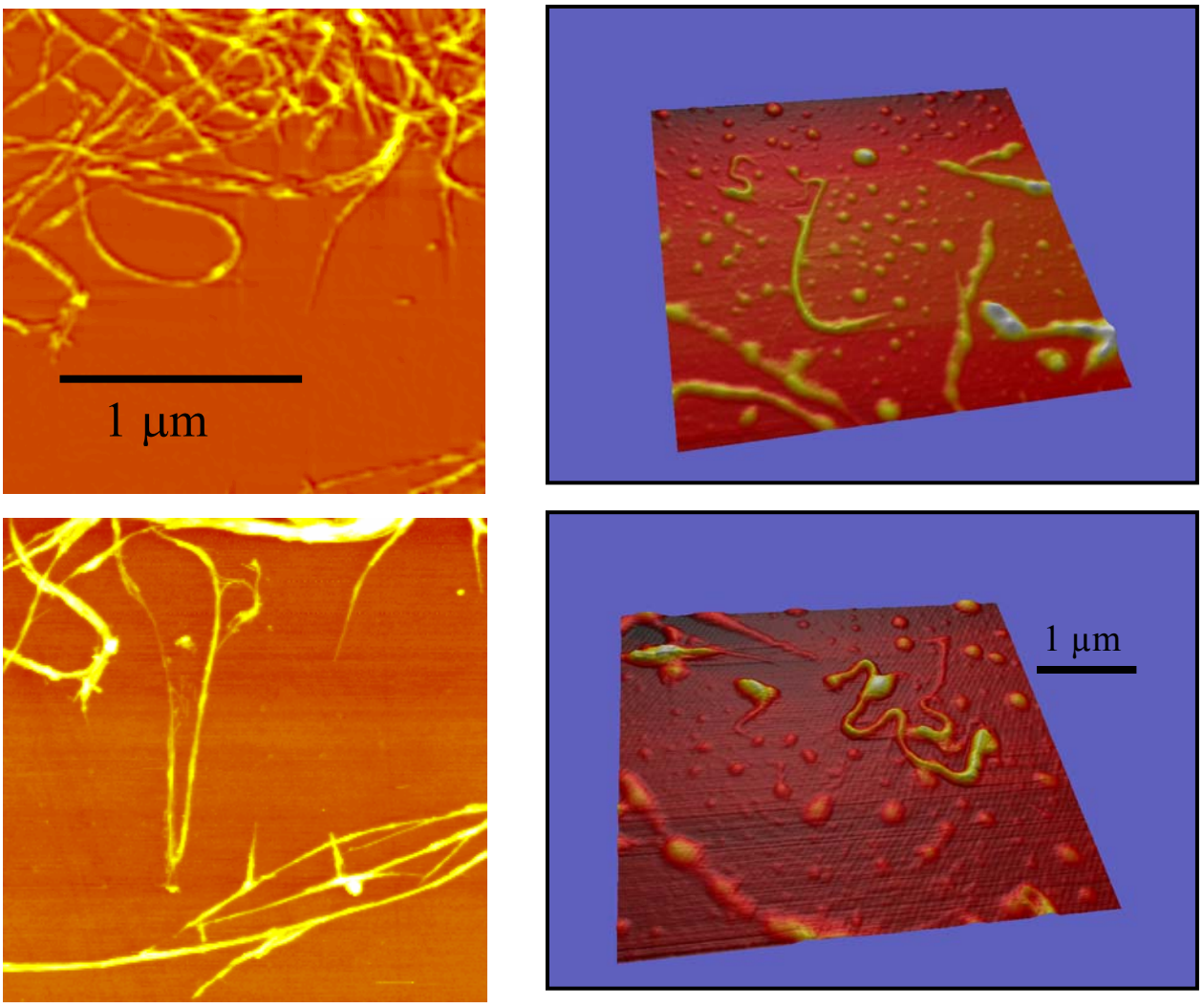

Figure 4.3 *- Left images from DI multimode IIIa AFM showing before and after of large CNT rope by direct manipulation using the AFM probe. Right, Nanomanipulator® images at different times during same session. The bottom pictures shows tubes manipulated to spell "NASA."*

4.2 Self Assembled Monolayers

Recent reports have demonstrated the ability to manipulate CNTs on a substrate and move them over relatively sizable distances [27, 28]. Originally, the findings in these reports were to be employed to use the Nanomanipulator® to move near-by, randomly deposited CNTs into contact with a set of electrodes completing a circuit with a CNT. This was quickly found to be impractical due the unreasonable time required to construct a single device, the inability to scale up fabrication, and the expense of operating the equipment. These factors necessitated an additional CNT positioning and deposition method which became the dielectrophoresis method discussed in detail in chapter 2 and the patterned self assembled monolayer (SAM) method described below.

In recent publications, it has been shown that self-assembly techniques offer a great potential for the positioning of CNTs [29, 30]. CNTs can be immobilized on a surface via electrostatic interactions between the nanotubes and surface-bound moieties. The strength of this interaction greatly depends on the nature of the terminal groups on the substrate. Silicon wafers are typically coated with a thin layer of either methyl- or amino-terminated groups using self-assembly techniques. CNTs have previously been shown to adhere strongly to amino-terminated surfaces and weakly to methyl-terminated surfaces. Combining these two observations leads to a scheme for CNT placement and alignment on a substrate.

Studies were conducted to determine the effects of CNT manipulation on functionalized SAM-coated Si substrates [31]. It has previously been shown that multi-walled CNTs, can be easily displaced or strained using the Nanomanipulator® without significant distortion of the nanotube topography [28]. According to M.R. Falvo et al., [27] the multi wall CNTs are much

stiffer and respond to the increased tip-to-sample force by rolling and then sliding. The same instrumentation can also be applied to the positioning of SWCNTs. Using the Nanomanipulator® interfaced with an Explorer SPM (ThermoMicroscopes), modifications were made to CNT ropes on different surfaces using a Nanodevices magnetic force cantilever operating both in tapping (imaging) mode and contact (manipulation) mode. The magnetic force probes were chosen because they are typically longer cantilevers having a lower spring constant than the typical non-contact tips used for general imaging. This allows greater control over the tip-surface force in the lower ranges used in moving CNTs. The stiffer tips simply cut, flatten or fray the CNTs instead of pushing them. Lateral force manipulation measurements were taken in the direction of a left to right line scan only.

During CNT manipulation testing, it was found SWCNTs are difficult to move while maintaining the integrity of the CNT ropes, which vary in length and diameter. Difficulties lie in the resolvable size and inter-dynamics of the CNT ropes. In this case, CNT ropes (3-15nm diameter) composed of several SWCNTs (averaging 1.4nm in diameter) respond differently to the direct force applied by the SPM tip than the multi-wall CNTs reported in reference [27].

Application of force by the SPM tip to the ropes normal to their long axis, yields different deformations on each of the different SAMs. After each modification of the surface/rope the sample was imaged. On the CNT repulsive trimethylsilyl (TMS) surface, ropes were deposited by spraying dispersed tubes on the substrate. Ropes on this surface ranged 5-15nm in diameter. Deformation of the rope typically followed a pattern consisting of an initially large lateral force which is maintained for a distance of approximately 300 – 500nm, followed by a decay period after which the lateral force returns to its zero state. On 3-aminopropyltriethoxysilane (APTES), tubes would quickly adhere to the surface when the substrate was immersed in a toluene solution

containing dispersed CNTs. The CNT ropes on this surface were on average smaller in diameter ranging from single tubes up to 8nm in diameter. Manipulations were conducted on larger CNT ropes to increase the signal- to-noise ratio. Manipulations differed from the TMS sample by having a shorter duration of the initial force and little to no decay period on the average manipulation. Figure 4.4 displays lateral force measurements for tube movement on APTES and TMS SAMs.

In addition to the differences in the modification data, the post-modification images taken on each sample show significant differences in how the CNTs move. On TMS, large portions of the tube were displaced, as opposed to the APTES samples where tube movement is localized to the area directly in contact with the probe tip. The surface modifications corresponding to the lateral forces depicted in the bottom of figure 4.4 are shown in figure 4.5 and are typical results for SWCNT ropes deposited on an APTES surface. Due to the labor intensive nature and the minimal advantage gained by the use of the SAMs for the controlled deposition of CNTs, this methodology for positioning CNTs is not practical for device development. This exercise, however, has further verified the feasibility of manipulating SWCNTs using an AFM, and has provided valuable insight into testing procedures and parameters which can be used for further CNT manipulations using the AFM / Nanomanipulator®. In particular, the lessons learned here regarding instrument settings and configurations have been directly applied to the work described in chapter 5.

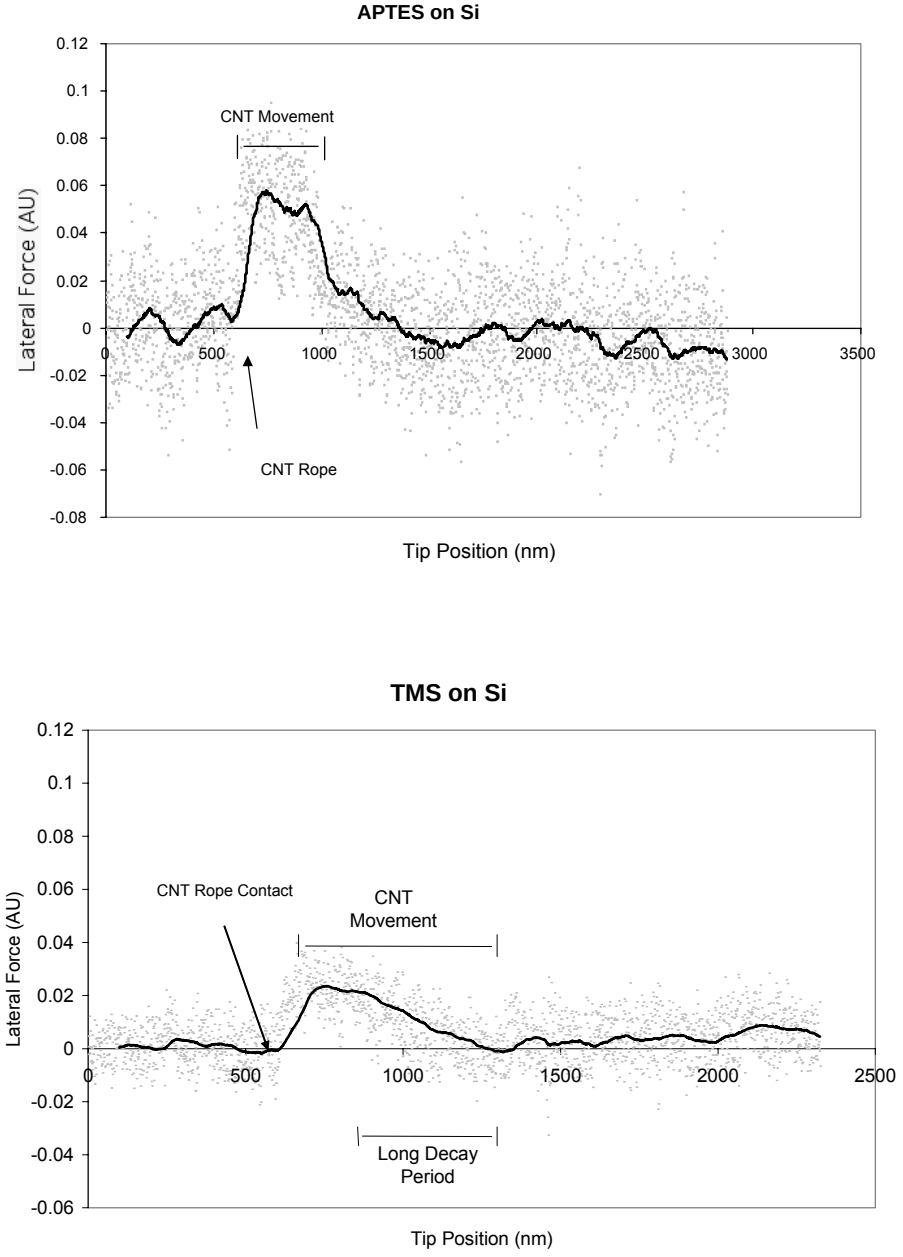

Figure 4.4 *- Lateral force data from CNT modification, APTES above and TMS below. Note the lower force and long decay in TMS data [31].*

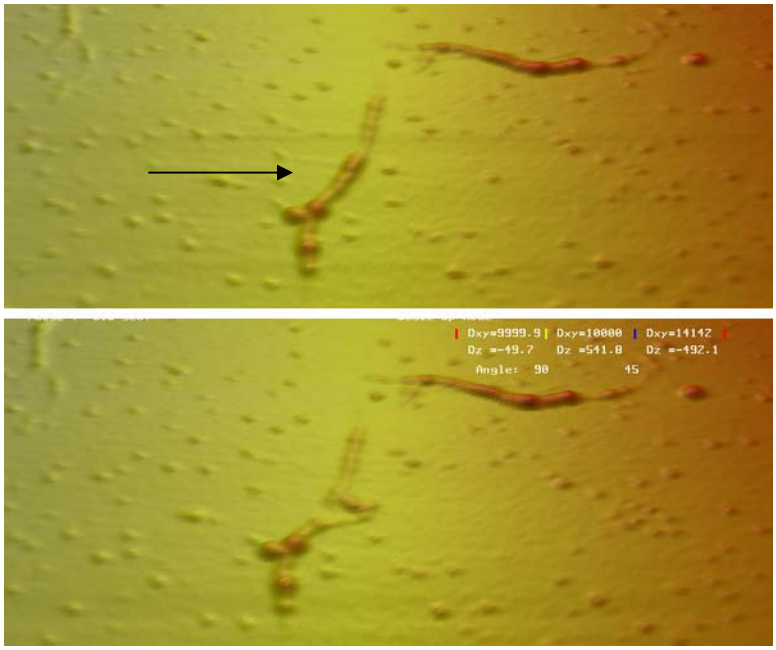

Figure 4.5 *- CNT rope on APTES coated wafer. Tip path is indicated in top picture. The resulting modification can clearly be seen in the post-modification image above [31].*

Additionally, by utilizing some of the knowledge gained from the SAM work above, an alternative CNT deposition methodology was discovered. By combining the principles of DEP described in chapter 2, the electron beam lithography methodologies in chapter 3, and the self-assembled monolayer work reported above, a method has been developed which consistently produces aligned CNTs between two electrodes in user defined locations. A detailed description of the development of this new methodology can be found in references [10, 32].

A diagram of the device used for testing is shown in figure 4.6 which uses the previously defined photolithography methods for fabrication. What makes this process unique, is the use of

an APTES SAM discussed earlier in a patterned location between the electrodes also shown in figure 4.6.

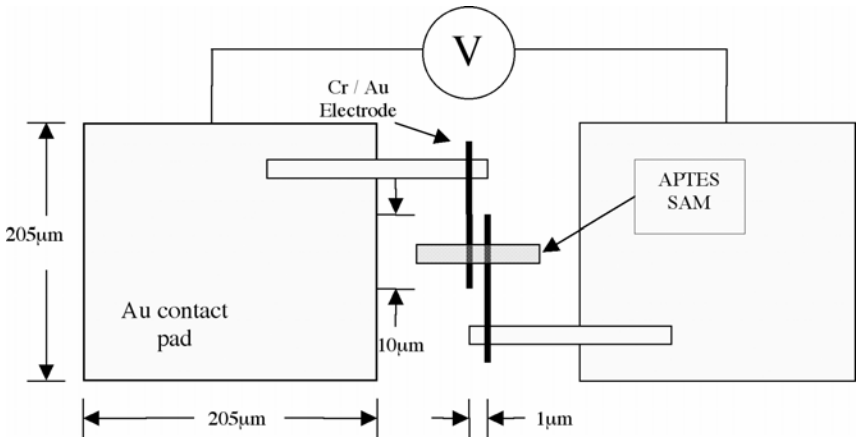

Figure 4.6 **-** Diagram of simple CNT circuit with Cr / Au contact pads and electrodes fabricated by basic photo and e-beam lithography methods [10].

The results of this experiment are shown figure 4.7. The CNTs align just as before with DEP. However, there is the added bonus of being able to precisely define locations on the surface where the CNTs are desired. The limiting factor in deposition precision is the electron beam width. Using this methodology, it should be possible to achieve SAM patterns with features less that 60nm in size which can be used for precision CNT deposition. This discovery may be important in future work were stray CNT may short out other circuits on a device or cause other unforeseen problems.

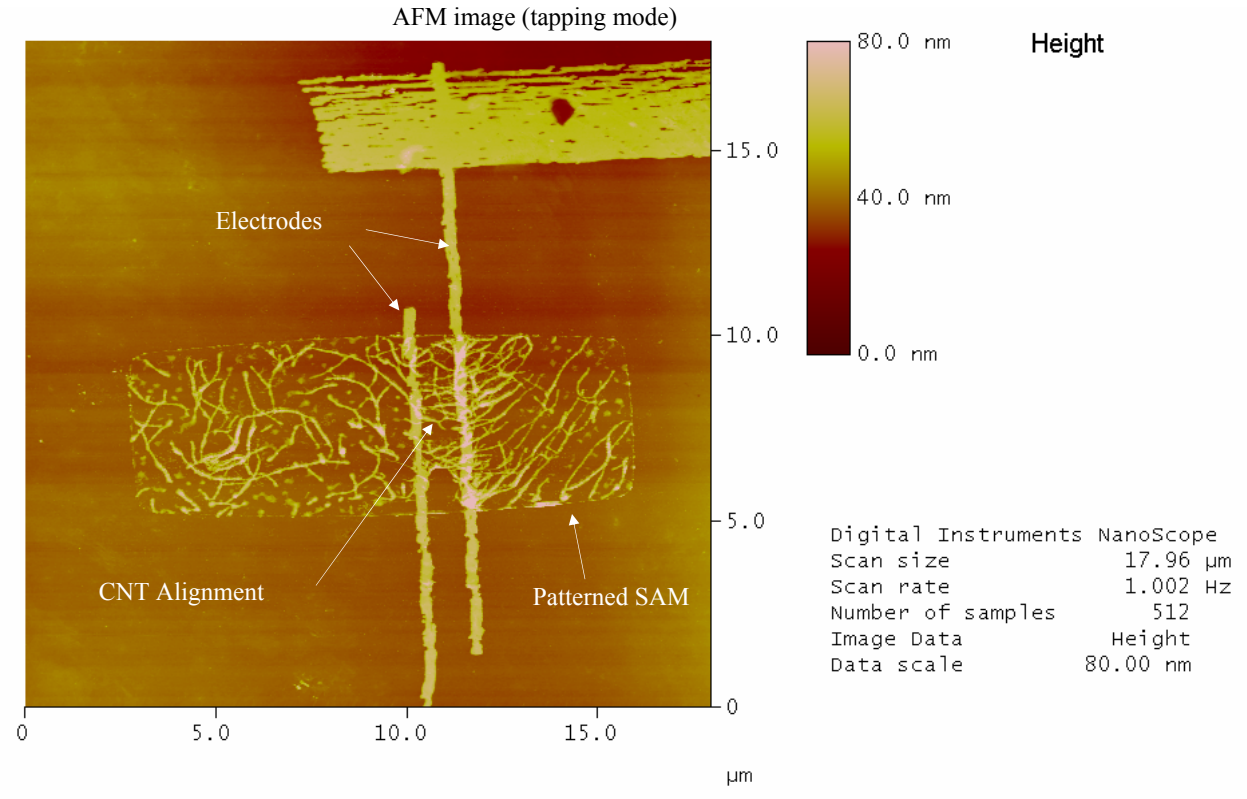

Figure 4.7 *- Patterned SWCNT deposition shows alignment of CNTs along the applied field lines in-between the electrodes with CNTs only located inside the patterned SAM region [10].*

Chapter 5: Experimental Setup / Strain Testing Results

Experimental studies are performed using the following sample preparation methods. Purified SWCNT material from Carbon Nanotechnologies, Inc. is used as received and suspended in electronic grade toluene at approximately 1μg/ml. The CNT solution is then sonicated for a period of 24 hours at which time the solution appears to be optically dispersed. The CNT solution is deposited on the surface of the samples and aligned between the electrodes using the di-electrophoretic technique described in chapter 2. This technique applies 10Vpp between opposing electrodes alternating at 5Mhz for 15sec. Then the sample is blown dry with nitrogen. The quantity of tubes deposited and aligned between the electrodes can be influenced by both the deposition time and the density of tubes in solution. It was found, however, that the previously mentioned parameters yield few CNT bundles aligned between the electrodes, often only a single bundle.

To facilitate CNT depositions and *in situ* conductivity measurements inside the atomic force microscope (AFM), the samples have been designed to fit inside a zero insertion force (ZIF) connector with pin outs for each individual circuit element. Using the ZIF connector for CNT deposition typically yields a better connection to the electrodes than using a point probe technique and results in a more even CNT distribution between the electrodes. The same FIZ connector is also used to *in situ* conductivity measurements.

Imaging and manipulation of the CNTs is done using the ThermoMicroscopes Explorer AFM coupled with the Nanomanipulator®. The sample is first imaged in tapping mode where a specific CNT bundle is identified for manipulation. Once engaged for manipulation the tip

travels a user-defined course in contact mode with a preset tip setpoint. The setpoint defines how much force this tip exerts on the sample surface. Typical setpoint values used ranged from .1-1 nanoAmps. To permit greater tip - surface force, stiffer Tap 300 cantilevers (NanoDevices, Inc.) were selected which have a resonant frequency of approximately 300Mhz. During the CNT manipulation, lateral force data are taken along with the CNT device resistivity data with a simple Labview program. Resistivity data are taken using an LR-700 linear resistance bridge while lateral force data and topography data are taken directly via the AFM. The experimental schematic is shown in figure 5.1.

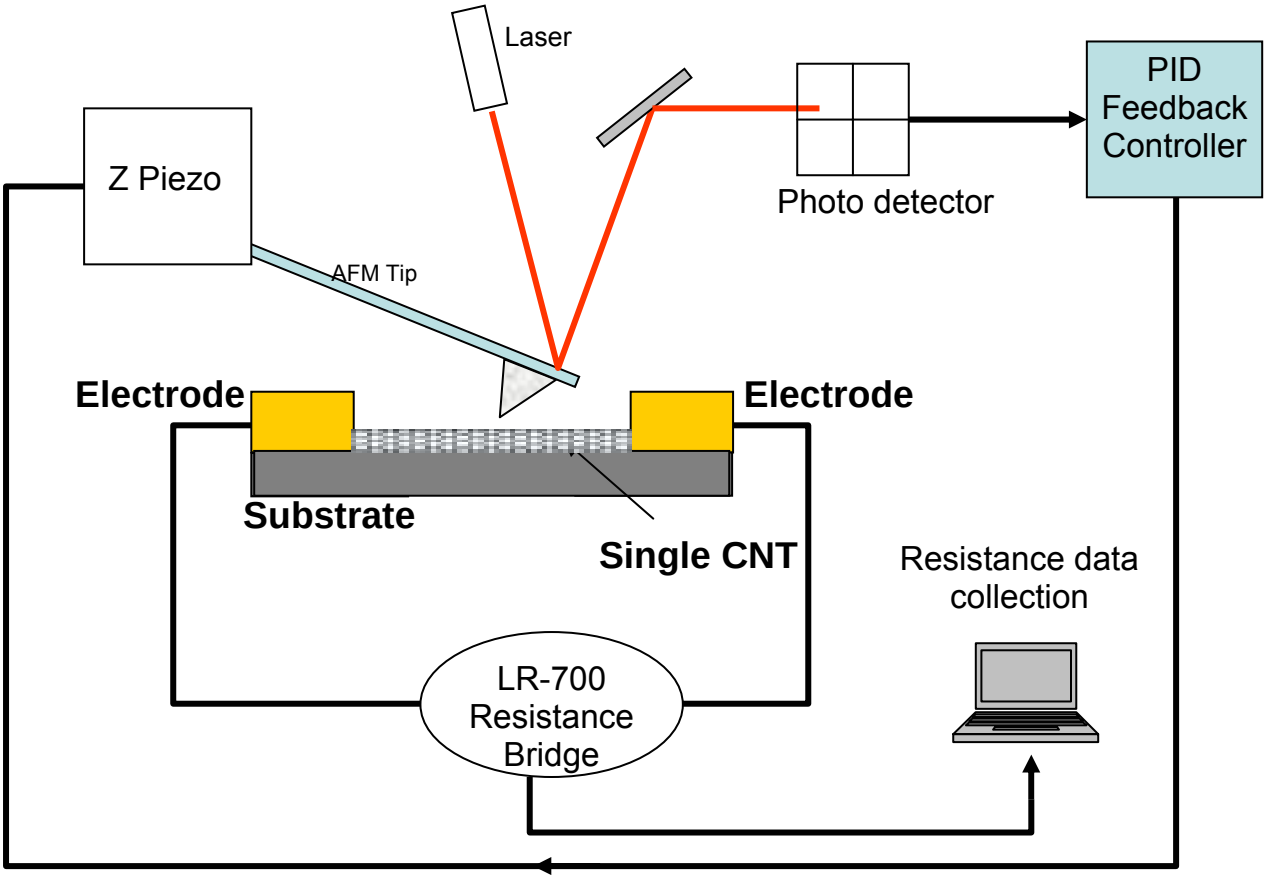

Figure 5.1 *- Experimental schematic showing the AFM / Nanomanipulator® and data acquisition configuration.*

On the sample shown in figure 5.2, three different bundles span from one set of electrodes to the other and result in several possible current carrying configurations. Two different paths were identified to be the most probable current carrying paths and were then tested with the Nanomanipulator®. The AFM tip is set close to the CNT, moved away from it, then through it, then back in the original direction. These direction changes are used to demonstrate a baseline measurement in the lateral force data shown in figure 5.3. The lateral force data also show the effect of the cantilever tip interacting with the nanotubes also shown in figure 5.3. By sweeping the cantilever across the surface in contact mode perpendicular to its long axis, the tip is sensitive to tribological forces on the surface. The sensitivity is represented as the twisting of the long cantilever using the tip at the end of the cantilever as a moment arm. The torque is measured in the photodetector by subtracting the right signal from the left signal illustrated in figure 5.1.

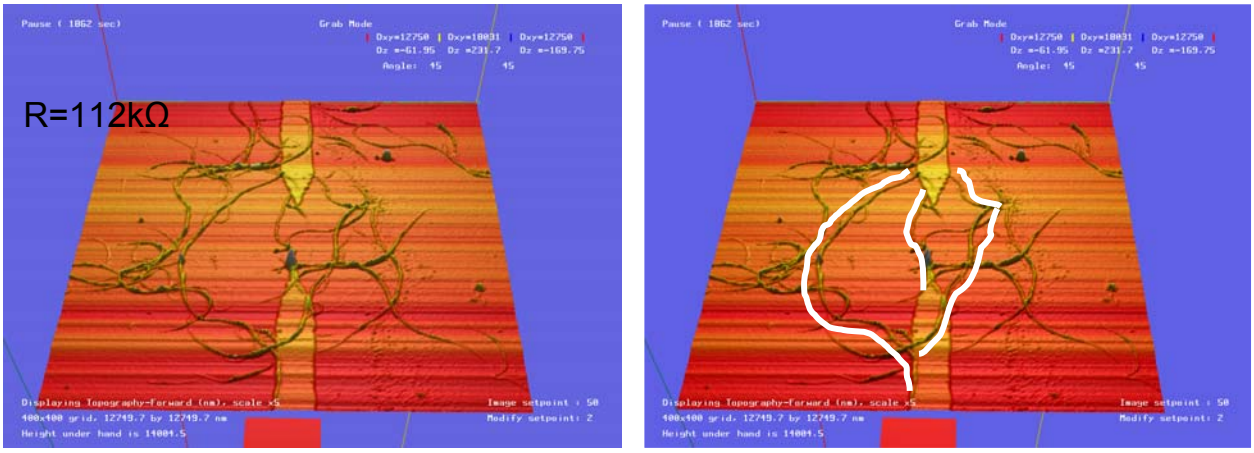

Figure 5.2 *- Nanomanipulator® image of the CNT device with nanotubes dispersed on the surface. There are three possible current carrying paths which have been identified and are outlined on the right image.*

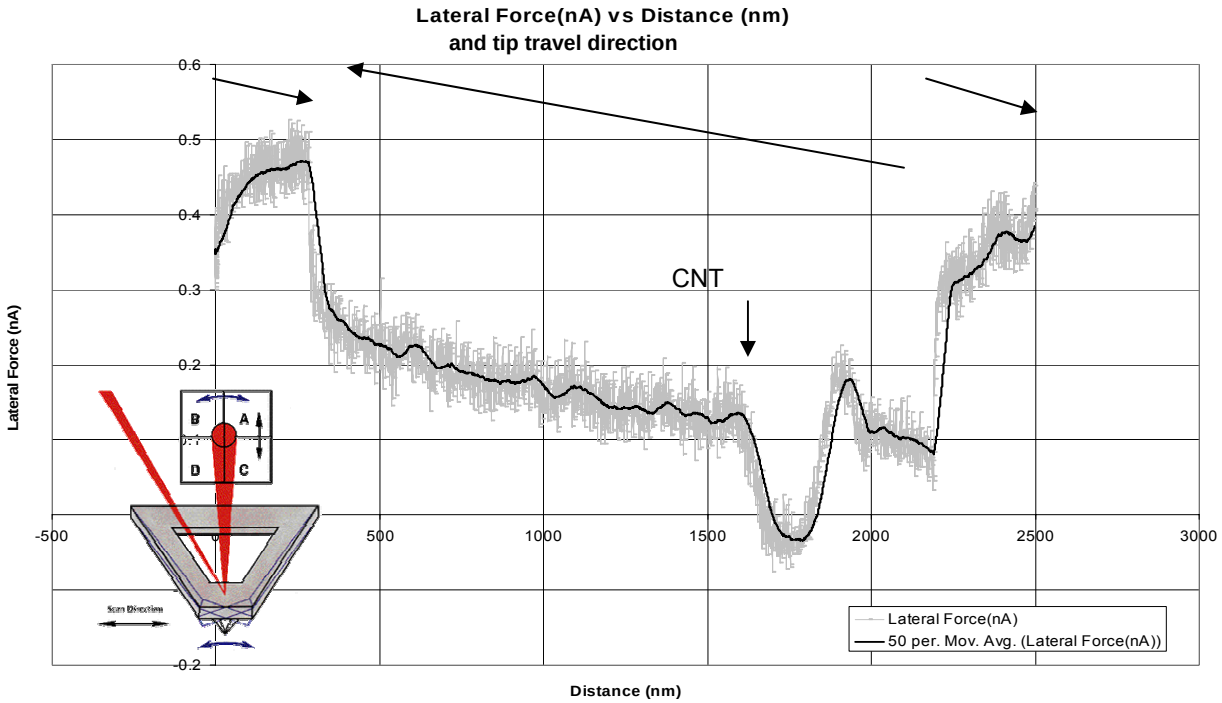

Figure 5.3 *- This is a typical lateral force curve for CNT manipulation. The arrows on the top of the chart indicate the direction the AFM tip was traveling while the LFM data was taken. The dip in the later portion of the data indicates the additional resistance of the CNTs interacting with the AFM cantilever.*

Fig. 5.4 shows the first CNT bundle selected to be moved in the left image and post manipulation in the right image. This modification, however, did not have any observable effect on the resistivity of the sample. The other probable current carrying CNT was then manipulated as shown in figure 5.3. This resulted in a slight displacement of a short portion of the CNT and a resistance change from 100kOhms to 127kOhms.

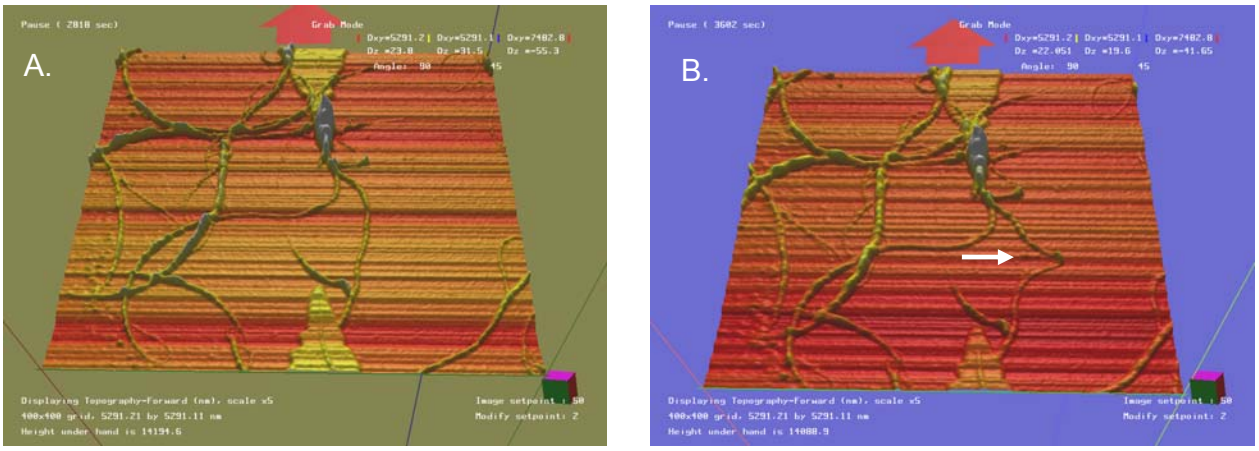

Figure 5.4 *- Nanomanipulator® screen image of the irst CNT bundle selected to be moved on the left and post manipulation on the right. This modification did not affect the resistivity of the sample.*

Of particular interest is how the deformations are highly localized to the portion of the tube that was in direct contact with the AFM tip and the immediate surrounding area. The full bundle does not move due to the strong van der Waal attraction between the CNT along its entire length and the SiO_2 surface of the substrate.

Further manipulations are shown in figure 5.5. An additional manipulation pushing the same CNT bundle further in the same direction results in a greater increase in the electrical resistance as shown in figure 5.5, manipulation 2. In manipulation 4, the same bundle was then pushed in the opposite direction (back towards its original position) resulting in a decrease in the resistance. This data suggest that the first manipulation strained the nanotubes. Then they were strained even more in the second manipulation, followed by the fourth manipulation which effectively relaxed them.

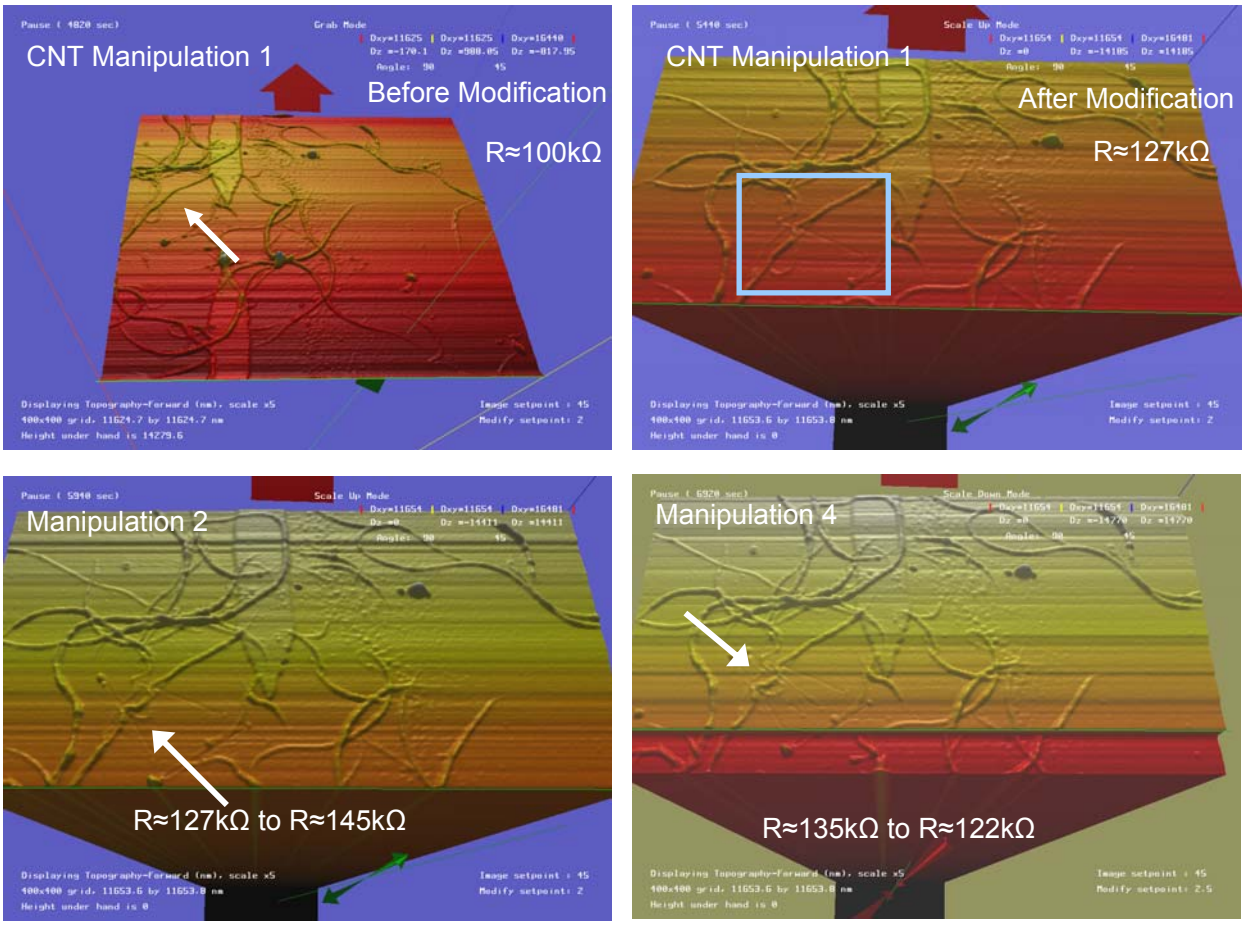

Figure 5.5 *- The CNT rope shown above left is now selected to be moved with the Nanomanipulator®. Above right shows the effect of the modification. The bottom two images show two different modifications of the CNT rope and their associated change in resistance.*

On the third manipulation, the AFM tip bounced over the CNT bundle and did not move it. This had little effect on the resistance of the device, and appeared in the data as a spike in the resistance as the probe moved over the bundle. The resistance vs time data are shown in fig. 5.6 along with the manipulations correlating to the changes in resistance.

While the AFM image of manipulation 5 is not included here, its effect is recorded in the resistance data in figure 5.6. This manipulation occurred on the same CNT rope as the previous

four manipulations but in a location closer to the upper electrode where no other manipulations had previously taken place. As shown in the data, this had a great effect on the resistance of the sample, and rapidly increased the resistance from about 120kΩ to more than 140kΩ.

The actual data in figure 5.6 are displayed in grey, and a 100 point moving average is shown in black. The slope seen at each of the manipulations in the moving average is an artifact of the averaging scheme.

A detailed discussion of these results follows in chapter 7.

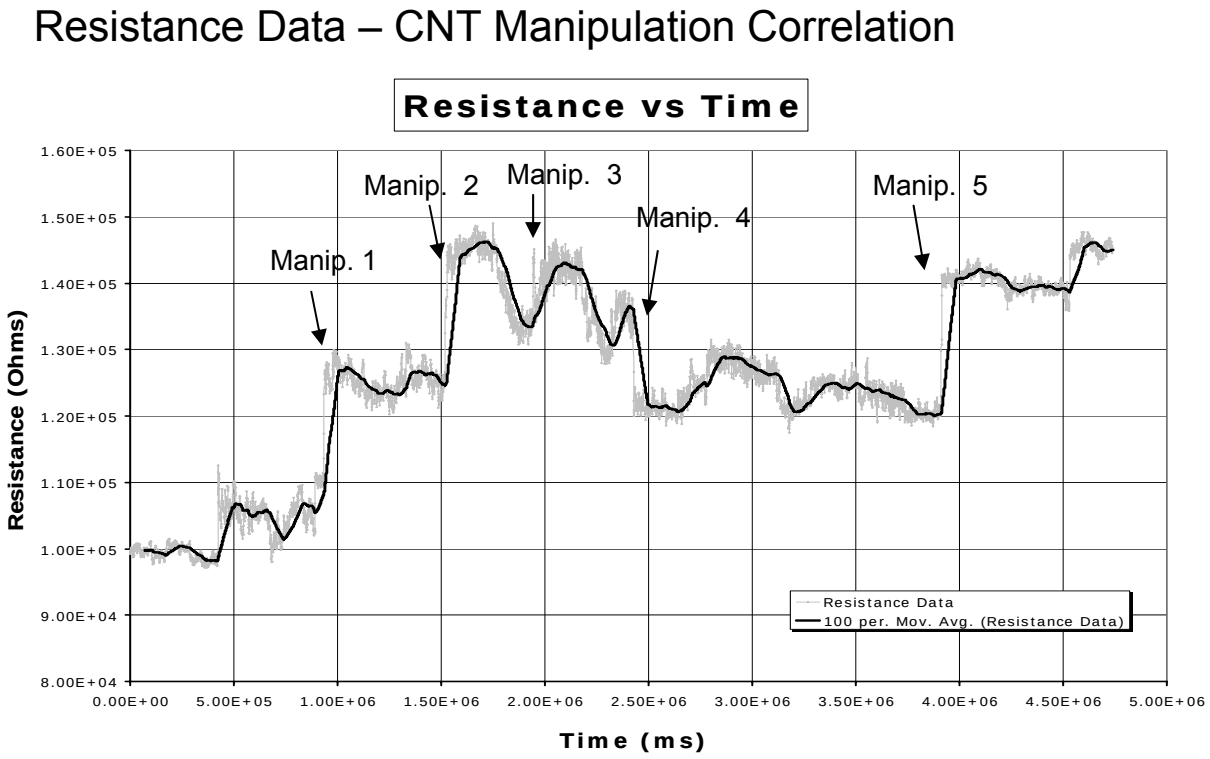

Figure 5.6 *- Resistance vs. Time data showing the correlation between CNT manipulations and resistance changes.*

Chapter 6: Flexible CNT-Based Strain Sensor

6.1 Device Fabrication

In order to apply uniaxial strain to nanotubes while monitoring their conductivity, a flexible strain sensitive nanotube-based device has been fabricated using the lithography techniques described in the previous chapters. Instead of having localized deformations caused by direct contact with an AFM tip, here the flexible nature of the polyimide on which the circuit is constructed transfers loading directly to the nanotubes.

Fabrication of the device begins first by coating a Si wafer with a polyimide. After the polyimide has cured on the surface, the sample can undergo the same lithography, metallization, and nanotube deposition steps described in previous chapters. Once completed, the polyimide can be separated from the silicon substrate by etching the oxide layer off the silicon, which yields the highly flexible CNT based circuit demonstrated in figure 6.1. Controlled strain vs. resistance testing is accomplished by mounting the flexible device to an aluminum coupon which is loaded in tension in a single axis load frame.

Detailed fabrication steps are as follows: toluene (ACS reagent grade, 99.5%), hydrofluoric acid (HF, 48% in water), sulfuric acid (H_2SO_4, ACS reagent grade), and hydrogen peroxide (H_2O_2, 30%) were purchased from Aldrich and used as received. Rapid-curing polyimide precursors solution (PI2525 and HMD 2610) was purchased from HD Microsystems and used as received. Oxidized silicon wafers (500 nm SiO_2 thickness) were purchased from TTI Silicon.

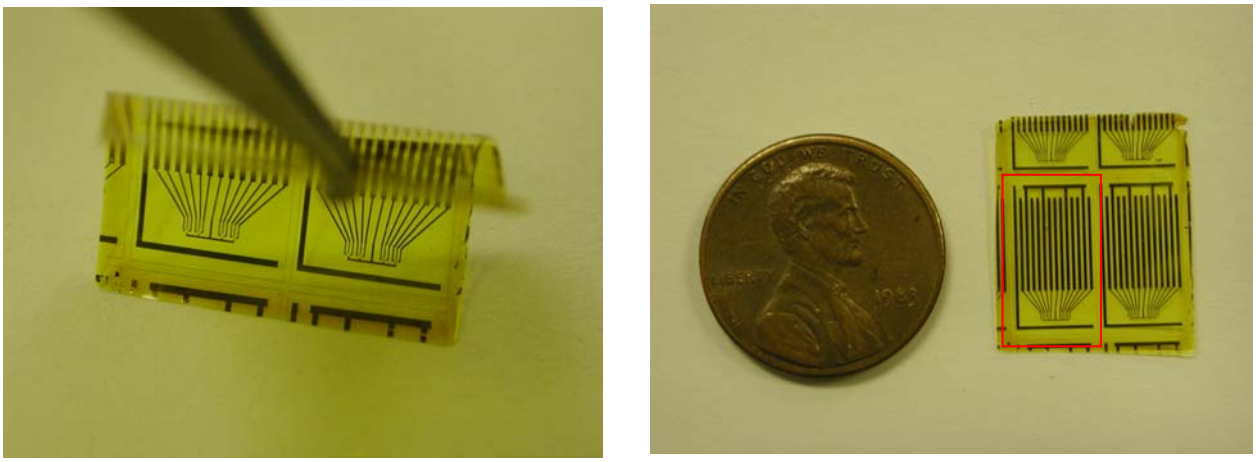

Figure 6.1 *- Flexible CNT-based strain sensor prototype.*

Before use, the oxidized silicon wafers were cleaned by immersion in "piranha" solution, 70:30 H_2SO_4:H_2O_2, for 30 minutes at 100°C to remove any organic contaminants present. After cleaning, the wafers were sequentially rinsed with de-ionized water and ethanol and then dried under a stream of nitrogen.

Prototype sensors were constructed on the flexible, plastic substrates by coating a cleaned oxidized silicon wafer with a thin film (~12 μm) of polyimide (PI2525) by spin coating at 2000 rpm for 30 seconds. After spinning, the film was cured in air by heating to 200°C at 4°C/min, holding at 200°C for 30 minutes, heating to 300°C at 2.5°C/min, and holding at 300°C for 60 minutes, followed by a gradual cooling to room temperature [33]. All patterning and SWCNT deposition was performed using the procedures listed for sensor fabrication in chapter 3.

Here, traditional photo- and electron-beam lithography and metal deposition techniques were used to deposit circuit elements followed by SWCNT deposition on the polyimide coated substrate. Large circuit elements (e.g bond pads, wires, etc.) were defined by illuminating with UV through the same photomask used for the Nanomanipulator® experiments. Following

development of the photoresist, a thin layer of gold (30 nm) was evaporated onto the surface. A set of electrodes was then defined using electron-beam lithography to deposit and align the SWCNTs using the same parameters as in section 3.1. To create electrodes for depositing and aligning the SWCNTs (or alignment electrodes), a thin layer of poly methyl methacrylate (PMMA) was deposited onto the pattern by spin coating at 3000 rpm for 30 seconds followed by a 90 second pre-bake at 180°C. The electrodes were then defined using an electron beam set to 20pA of beam current and a beam dose (line dose) of 1.3 nC/cm. The typical width of each electrode was approximately 1 μm, and the separation between the electrodes was 3 μm.

Deposition and alignment of the SWCNTs was accomplished using a dielectrophoretic technique. First, a small amount of nanotubes, approximately 1μg/ml, was dispersed in toluene by ultrasonication for 24 hours. Because the concentration of nanotubes in the suspension was small, only a slight discoloration occurred when inspected optically. Several drops of this solution were then placed on the sample so that the electrode surface was covered. Two spring-loaded pins were then used to make contact with the pads for the dielectrophoresis CNT deposition and alignment. Typical DEP conditions for deposition were 10 V_{PP} at 2 MHz for 15sec.

Following the required lithography, metal deposition and CNT deposition steps, the polyimide film was removed from the silicon surface by dissolving the oxide layer on the Si wafer using a 1% hydrofluoric acid (HF) solution. To prevent the nanotubes from being dislodged during the removal process, the polyimide coated silicon surface was held vertically by forceps so that only one edge of the surface is exposed to the HF. As the HF dissolves the oxide layer, capillary forces draw the HF up behind the polyimide layer, resulting in removal of the

polyimide film while protecting the nanotubes from the HF solution. After removal of the film, the polyimide substrate is gently rinsed with de-ionized water to remove any residual HF [33].

6.2 Device Testing

Once fabricated and removed from the silicon substrate, the device was mounted onto the center of an aluminum strip with Micromeasurements GA-2 epoxy. Two strain gauges were also mounted to the aluminum strip with MicroMeasurements M-Bond 200 adhesive, directly opposite from the CNT device. One axial and one transverse gauge seen in figure 6.2 were used as reference gauges. The transverse gauge, however, was not used in this work.

The four CNT sensing elements of each device were wired in parallel and connected to the LR-700 resistance bridge. The resistance bridge sources current and measures the voltage drop over the sample. This can be conducted in a four lead measurement or a two lead measurement as was performed in this work. Knowing the voltage and current, it returns the sample's resistance.

Silver conductive paint was used to connect the device to the wire leads. The specimen was loaded into the single axis load frame shown in figure 6.2 and cycled through a variety of loading conditions. For each test, the resistance of each device was monitored and plotted against the strain data from the strain gauges.

The aluminum coupons on which the CNT samples were mounted were cyclically loaded at different ranges of loads between 2204 psi and 22040 psi at .01Hz. The load frame in this case was operated by controlling the loading in Newtons, pounds, or kilograms. The cross-sectional area of the aluminum coupon was measured and used to determine the loading in terms

of pressure in the aluminum in psi. These loads then translated to strains from 100 to 710 microstrain. The strain data are shown in figures 6.3 through 6.9.

Figure 6.2 *- Top left shows the polyimide CNT device mounted onto the aluminum strip. Each device is tested with all four sensing locations wired in parallel. Electrical connections to the device are made by using conductive paint to attach the leads. Tensile testing takes place in a single axis load frame shown right. Direct strain measurements were made with strain gauges mounted to the back side shown in the bottom left.*

Figures 6.3 and 6.4 show data collected from the load testing performed on sample 1. In figure 6.3, the resistance data follow the strain data very closely over the duration of the test. Some drift in the resistance data is observed but overall the resistance responds consistently to the applied load. Figure 6.4 is a close-up of figure 6.3 and shows how closely the resistance follows the applied load.

Additional tensile testing was performed on sample 1 over different load ranges from 450-725 microstrain. This is shown in figures 6.5 and 6.6. In each figure the resistance of the circuit changes with the application of load to the sample over all of the strains tested.

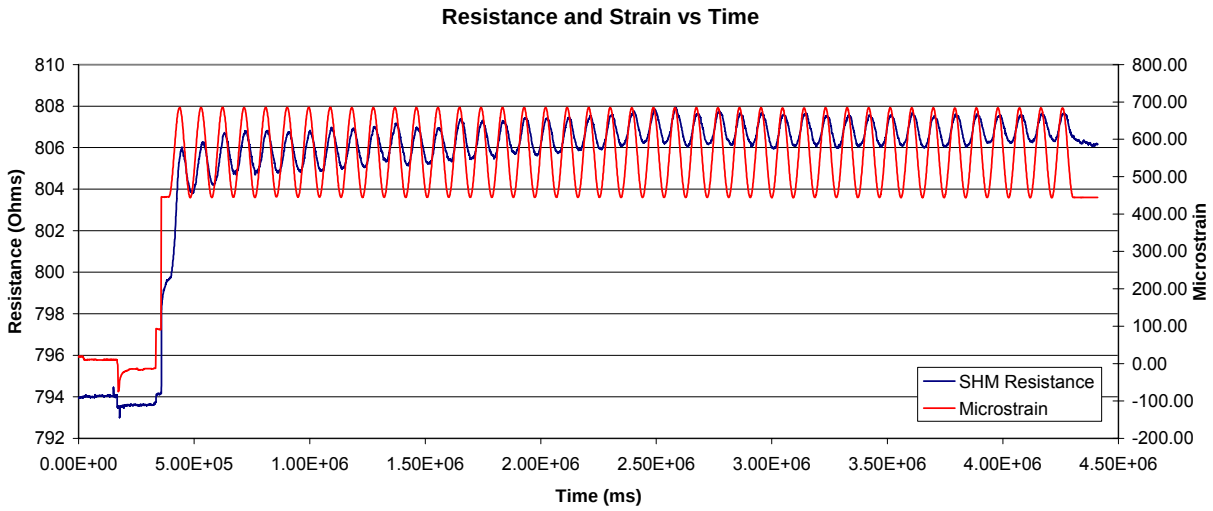

Figure 6.3 *- Sample 1 Load test datafrom 450 – 700 microstrain.*

Close up of Sample 1 Load Test

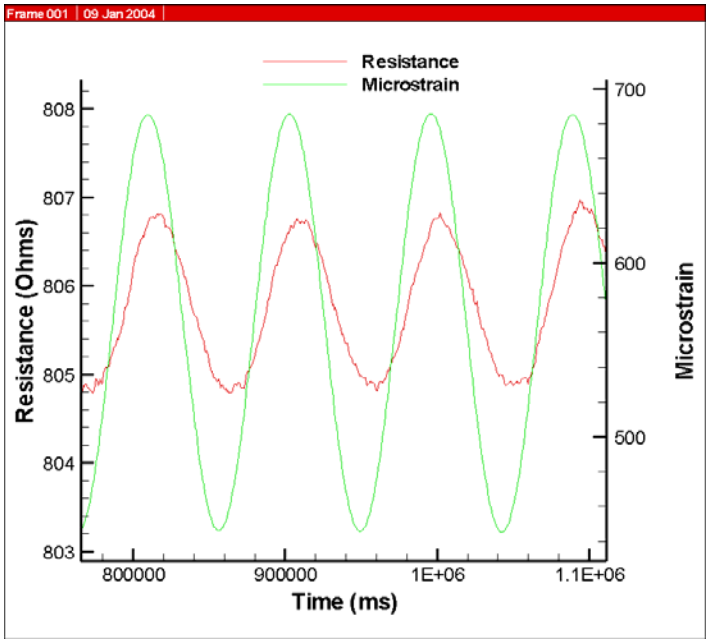

Figure 6.4 *- Sample 1 Load test data close up of figure 6.3*

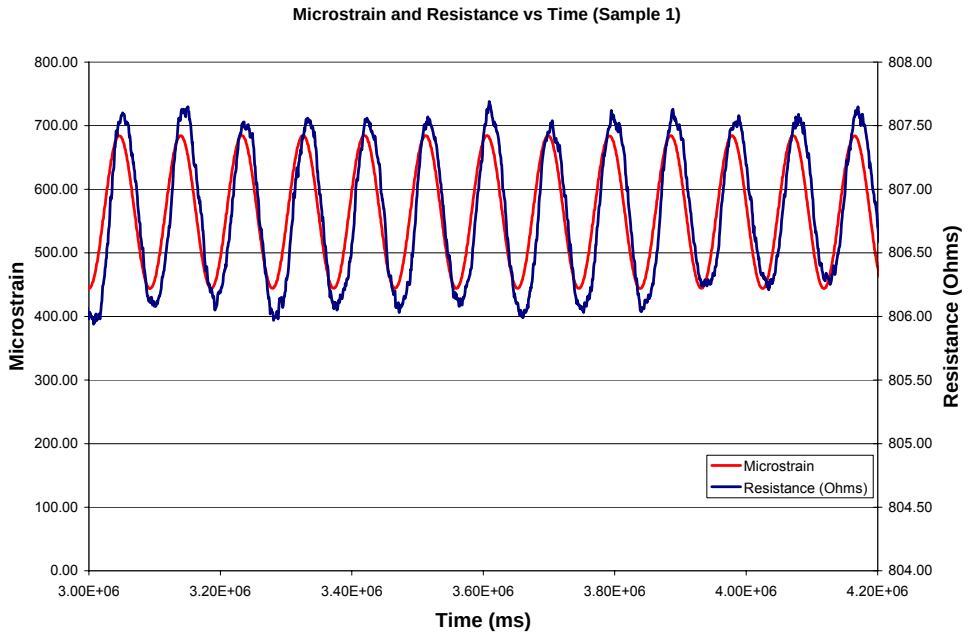

Figure 6.5 *- Sample 1 load test data at 450 – 700 microstrain.*

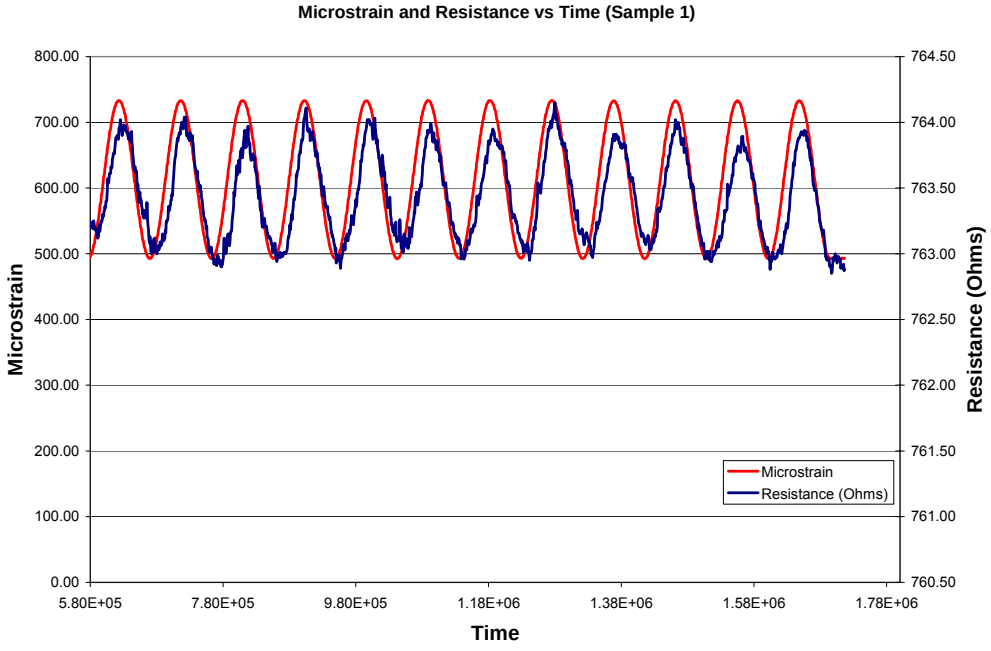

Figure 6.6 *- Sample 1 Load Test Data at 500-725 microstrain.*

Strain vs. resistance testing was also performed on a second flexible sample. This sample showed a much higher resistance before loading than sample 1. Where sample 1 had a resistance less than1kΩ, sample 2 showed a resistance of approximately 2kΩ. The decreased conductivity in sample 2 caused the resistance data to be noisier than that of sample 1. Figures 6.7, 6.8, and 6.9 show the resistance and loading data taken for sample 2. The testing in figure 6.7 included two different load tests run consecutively(before t=2.00E+06, and after t=2.00E+06.) The large change at approximately about t=1.4E+06 is thought to be caused by changes in ambient temperature and is discussed further in chapter 7.

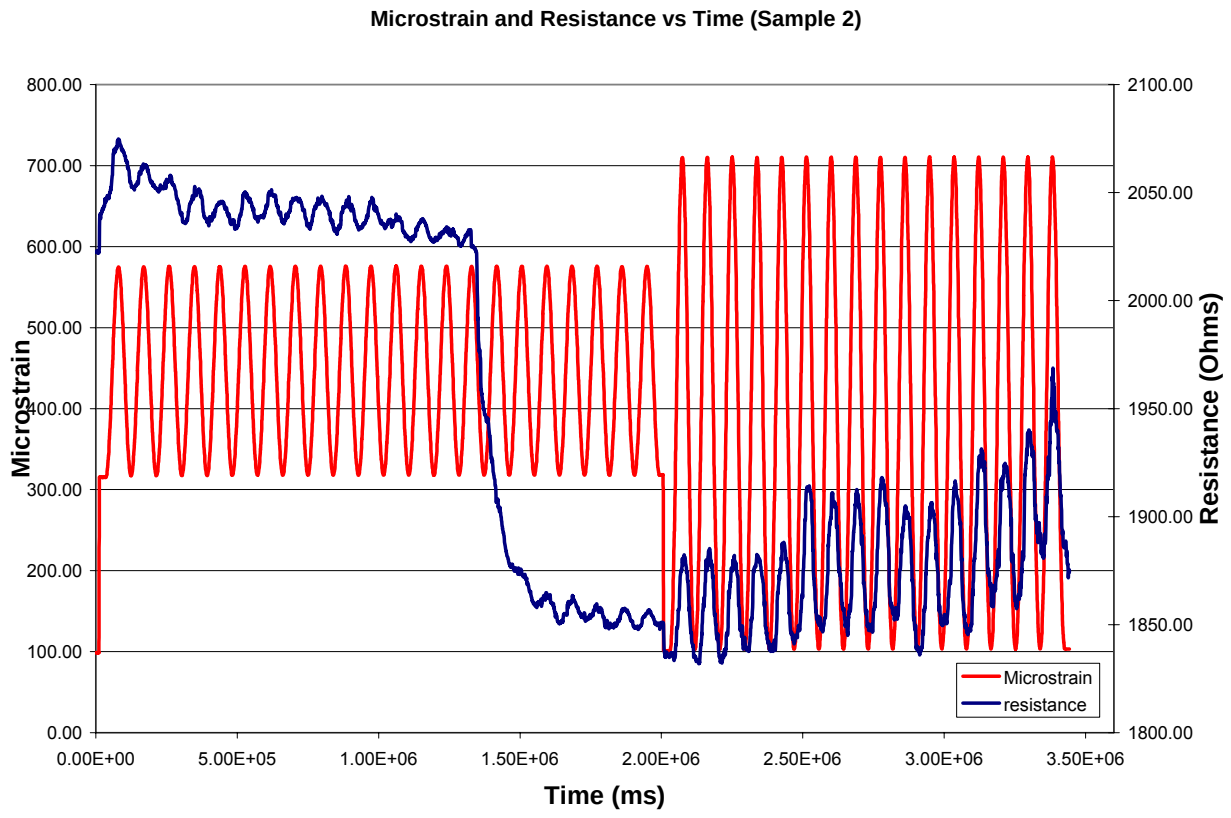

Figure 6.7 *- Load test data of Sample 2. Here loading is shown at two different amplitudes. Resistance follows the loading as expected. At about t=1.4E+06 ms the data takes a large drop. This effect was observed on other occasions while testing and is believed to an effect of temperature which was not measured here during this test.*

Figures 6.8 and 6.9 show each of these sections individually to more clearly show how the resistance is affected by the strain. As expected, the magnitude of the resistance change is higher under greater loading and can easily be observed in figure 6.7. The average change in resistance for the lighter loading case was approximately 15Ω where in the larger loading case, the average change was approximately 60Ω.

Further discussion of the data collected here and in chapter 5 follows in Chapter 7.

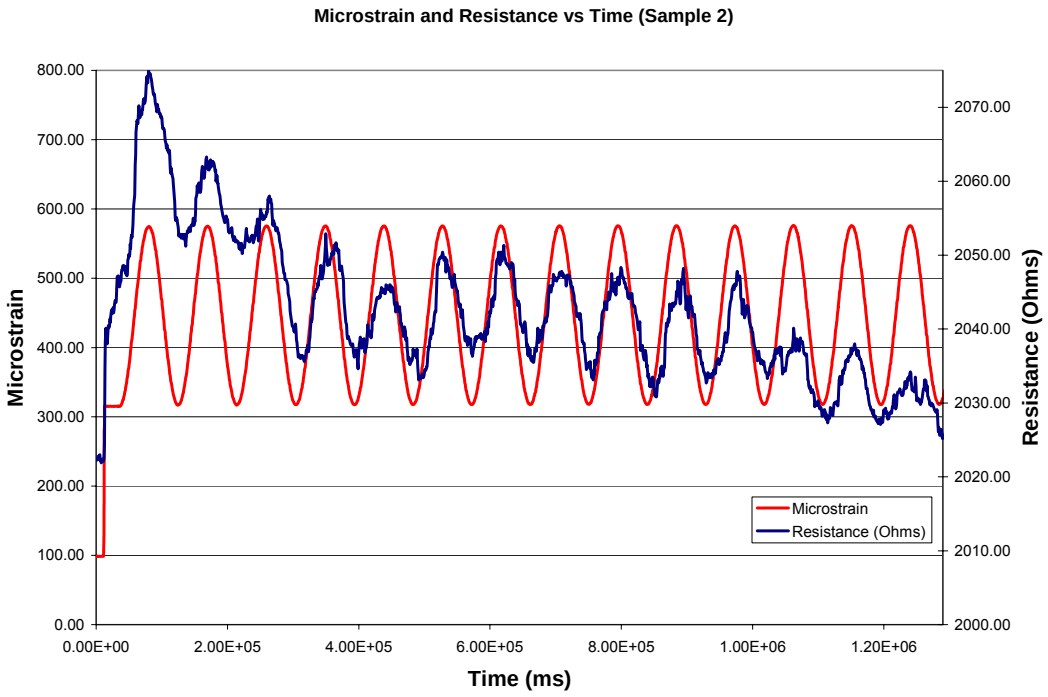

Figure 6.8 *- Sample 2 Load test data form 308 – 570 microstrain.*

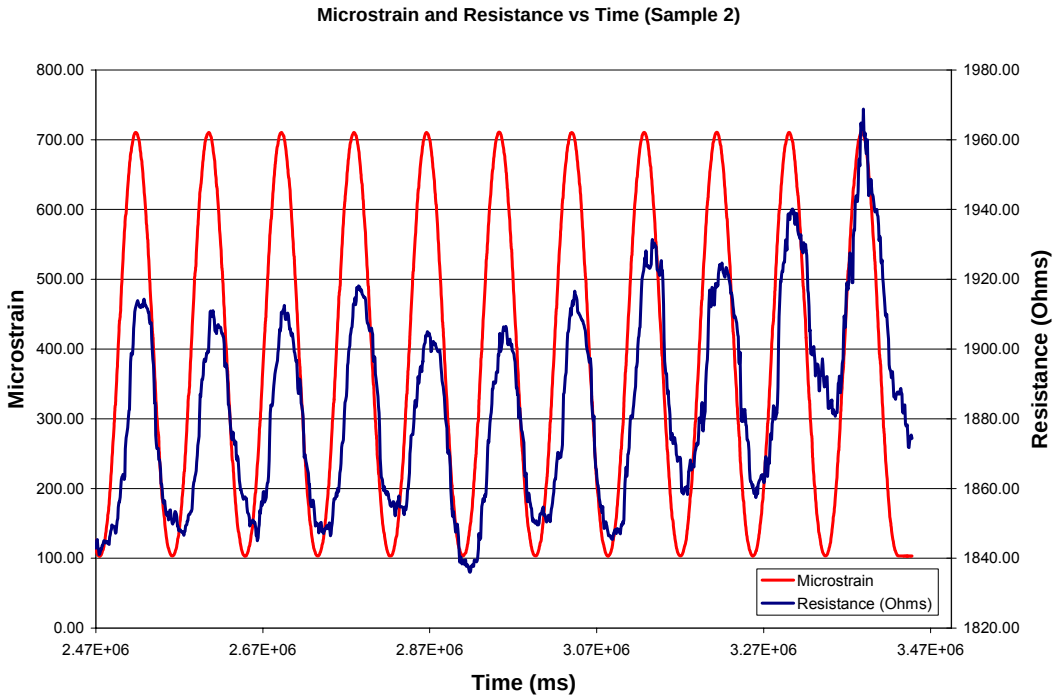

Figure 6.9 - Sample 2 Load test data from 100 to 710 microstrain.

Chapter 7: Discussion of Results and Future Research

7.1 Discussion of Results

Three major objectives have been achieved in this thesis. A theoretical prediction has been made which predicts forces exerted on twelve different species of SWCNTs under dielectrophoreis between two pointed electrodes three microns apart. The effect of localized deformations in CNTs on conductivity was measured using an atomic force microscope to strain the CNTs on a specially designed thin film circuit testbed. Finally, the effect of uniaxial loading of CNTs on their conductivity was measured by fabricating a flexible circuit which was mounted to a test coupon and cyclically loaded axially in tension.

Both the theoretical predictions in chapter 2 and experimental data presented in chapter 3 indicate that CNTs will align to the applied electric field lines. The finite element results from chapter 2 indicate the electric field lines produced by the patterned electrodes are highly consistent with CNT deposition and alignment images shown in figure 3.6. Additionally the predictions made in chapter 2 on the dielectrophoretic alignment of SWCNTs indicate that it is much more likely to draw metallic and small-gap semiconducting nanotubes in between the electrodes than it would be to draw semiconducting nanotubes. Since small-gap semiconducting CNTs are predicted to be the most sensitive to strain as discussed in section 2.2, this is a highly desired effect.

Experimental data confirming the alignment predictions have been acquired using several experimental designs. It is clear from the data presented in sections 2.1, 3.2, and 4.2 that the nanotubes are aligning to the applied electric field. However it is more difficult to determine the

composition of the deposited CNTs. One indication of CNT composition would be the resistance of the deposited CNTs. If the DEP is drawing mostly metallic CNTs, the resistance of the DEP deposited CNTs should be lower than for a random deposition of CNTs. With this in mind, conductivity tests were made on the sample shown in figure 3.7 which has two separate circuit locations on it: one with DEP deposited tubes and one with randomly deposited tubes. The sample on the right of figure 3.7 with the DEP deposited tubes showed a resistance of 10.5kΩ where as the sample on the left was open. Additionally, the DEP aligned sample shows significantly more nanotubes which have been congregated in the regions where the field gradients are the strongest, i.e., between the two electrodes. It is unclear if the lower resistance is due to the presence of mostly metallic nanotubes or to the fact that there are significantly more nanotubes which result in increased conductance paths to reduce the resistance of the sample.

The Nanomanipulator® study described in chapter 5 has successfully demonstrated the ability to fabricate and test a HiPCO CNT based strain sensitive device. Deformation of CNTs by direct manipulation while measuring the effect on electron transport clearly showed changes in resistance with strain. The results from this study confirm the resistive tunability of the CNTs and show that it is possible to fabricate a CNT based sensor from a bulk CNT suspension. These results provide very good incentives for pursuing further CNT based sensor research and, coupled with the alignment and deposition techniques described in chapters 2 and 3, the results offer a possibility for a large scale build up of CNT device production.

In this experiment, SWCNTs were aligned between two electrodes then deformed using an AFM tip while their electrical resistance was measured. The AFM tip was able to displace small segments of the CNTs near to where the tip made contact with the tubes. The rest of the tubes remained firmly fixed on the surface due to van der Waals forces. Each manipulation of

the CNT resulted in changes in the resistance as shown in figure 5.6. The first manipulation caused the resistance (R) to rise from 100kΩ (R_0) to 121kΩ. An additional manipulation displacing the CNT further in the same direction caused the resistance to further increase from 127kΩ to 145kΩ. The effect of the two manipulations on the CNT bundle is a total ΔR of 45kΩ or $\Delta R/R_0$ of approximately 45%. The Nanomanipulator® was then used to push the CNT bundle back towards its original position. The result of this manipulation was a reduction in the resistance from 135kΩ to 122kΩ. These results are consistent with a similar experiment conducted by Tombler, *et al.* [9] where individual nanotubes were suspended over a trench between two electrodes. Reference [9] relates localized deformations in the CNT structure to changes in conductivity caused by localized deformations developing in the carbon-carbon bonds within the nanotube from force applied to the tube by an AFM tip. With their experimental configuration, they were able to repeatedly deform CNTs at different magnitudes and allow them to return to their original resting states while monitoring the resistances of the CNTs. The main difference in the work presented here as opposed to that of Tombler et al. [9] is that the CNTs are bundles of HiPCO CNTs instead of single catalytically grown CNTs, and are fixed to the surface instead of being suspended. In the work presented in chapter 5, the nanotubes are attracted to the surface along their entire length by van der Waals forces. Since the AFM probe is so small at its tip, it only exerts a force over a very small length of the CNT bundle and it is able to displace only the region proximal to the tip. For this reason, only small deformations were possible when manipulating the CNTs.

Displacing the nanotubes with the AFM tip temporarily overcomes the van der Waals forces and is analogous to pushing the suspended CNTs in reference [9]. Once the nanotubes have been displaced, van der Waals forces dominate the nanotube – surface interaction and hold the nanotubes in their displaced state, not allowing them to recover from their deformation. This is shown in the AFM manipulation data in figures 4.3, 4.6, 5. 4, and 5.5.

After the two consecutive displacements, the change in resistance, ΔR of 45kΩ, is less than an order of magnitude and is consistent with the results in [9] which demonstrated a conductance change of approximately 50% for a strain of approximately 1%.

The mechanics of this displacement could be a combination of two different phenomena. The first, described in chapter 2, is the actual straining or elongation of the CNTs. The other phenomenon is that the individual tubes within the bundle slide very easily against one another and will slip to elongate when pushed by the AFM tip. This, too, could cause a change in the resistance due to the changing tube–to–tube contact.

Because of the CNT bundling, it is impossible to know what kinds of tubes are being strained in each sample. The electric current however will choose a path of the least resistance though the bundle which could be though both metallic and semiconducting CNTs. Since metallic CNTs are theorized to be the least sensitive to strain due to their high lattice symmetry, it is very likely that the strain – resistance effects observed here can be attributed to a small number of small-gap semiconducting CNTs. Thus, the localized deformation of the CNTs is consistent with molecular dynamics modeling presented earlier [9] which determined that the observed changes in resistance are due to localized changes in the carbon bonding hybridization.

The effect of uniaxial loading of SWCNTs on resistivity was measured by developing a flexible substrate on which a thin film CNT based circuit was constructed. The test results shown in figures 6.3-6.9 clearly indicate repeatable sensitivity to strain through the multiple samples tested. Since the samples were prototypes, and it was not known how the devices would respond as a whole to loading, only small strains were tested in this study.

The data shown in figures 6.3 through 6.9 indicate high strain sensitivity in the flexible polyimide CNT devices. The strains used in this test were significantly smaller than in the tests performed in chapter 5 as in well as the testing conducted in [9]. Both of the samples shown here demonstrate for each loading case that the resistance data follow the strain data very closely and have variations in the resistance at the same frequency used to load the samples. As expected, each sample increases its resistance when the load is increased, and the resistance decreases when the load is decreased.

Some samples, however, did not show any sensitivity to strain. In some cases the resistance of the samples was so large due to poor CNT-metal contact, oxidization problems in the metal deposition process, or poor CNT depositions, that variations in the resistance which could be attributed to strain were within the error of the measurement. Other samples simply did not conduct at all after fabrication was completed, victims possibly of electrostatic discharge or even something as simple as a scratch on the surface severing one of the delicate thin film metallic leads. Sensitivity varied between samples with a $\Delta R/R$ being usually $< 1\%$. The differences are attributed to the quantity and composition of nanotubes deposited on the device.

The height measurements of the different samples used in this thesis indicate that the nanotubes are highly bundled having 2-100 nanotubes in each bundle. Few samples showed signs of single nanotubes. Just as before there are a variety of nanotubes in each bundle. While

the metallic tubes are preferred in the alignment process, they carry along semiconducting tubes in their bundles. Again, the varying CNT composition and quantity account for the differences in resistance and sensitivity in the samples.

Load testing indicates a phase lag of 29 degrees between what is measured by the strain gauge and the resistance changes from the CNT sample as clearly seen in figure 6.4. This was originally thought to be caused by the plastic nature of the polyimide. However, a control test which placed a strain gauge directly on the polyimide and one on the back side of the aluminum coupon to which the polyimide was adhered showed good correlation between resistance cycles and loading as shown in figure 7.1. Importantly, no phase shift between resistance and loading was observed in this test as shown in figure 7.1. Only at frequencies above 5Hz was any noticeable phase difference observed and, as mentioned above, load testing on the CNT polyimide samples was performed at .01Hz. It is now thought that the phase shift is most likely caused by temperature differences at the sample location. While this was not known during the time of testing, later experiments on similar CNT based electro-mechanically sensitive materials did indicate a very strong sensitivity to temperature. Temperature measurements were made using a resistive temperature device (RTD) temperature sensor at a distance of 1cm away form the center of a coupon. The coupon was loaded under conditions similar to those used in this test and on the on the same load frame.

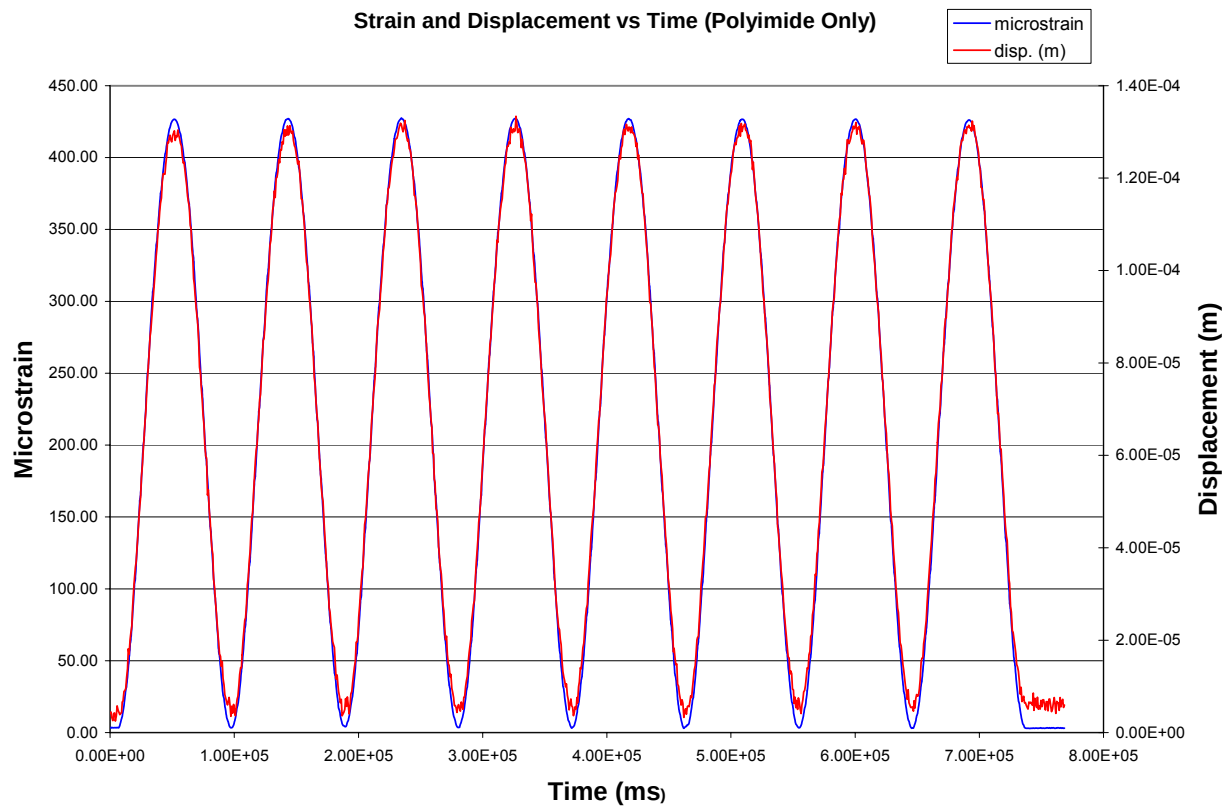

Figure 7.1 *- Polyimide load test data. Here a blank polyimide sample was mounted to a test coupon and strain gauges were mounted both on the polyimide as well as on the test coupon. This data demonstrates how the polyimide is able to transfer the load to the strain gauge though its thickness. The polyimide deformation follows the displacement of the load frame with a very high degree of precision.*

The data show slight temperature changes at the same frequency as the loading of the coupon. The exact cause of this temperature change is unclear; it is, however, lagged in phase by 69 degrees and shown in figure 7.2. Figure 7.2 presents temperature data taken on a blank aluminum coupon vs. displacement under similar load conditions to the CNT based samples presented here and is compared to figure 6.4.

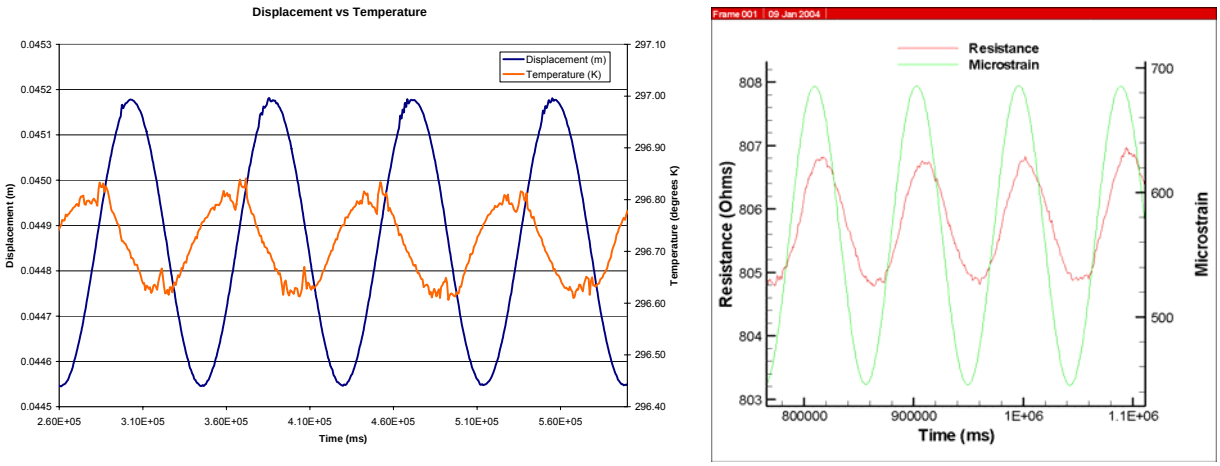

Figure 7.2 *- Temperature vs displacement of a loaded aluminum coupon used to test the flexible polyimide-CNT samples is shown on the left. Figure 6.4 is reproduced on the right for comparison. The temperature measurement at the aluminum coupon is opposite to the observed resistance change in the flexible CNT device.*

While the temperature measurement strongly resembles an inverse relationship to resistance, the strain is still believed to be responsible for the change in resistance. It has already been shown earlier that CNTs increase in electrical resistance under loading. Additionally the two measurements indicate a large difference in their phase shift; the temperature shifts by 69 degrees and the resistance by 29 degrees. This is a difference of 40 degrees or 11%. Since nanotubes are known to be one of the best heat conductors available, a more immediate response to the changes in temperature would be expected to result in little to no phase shift.

Another effect most likely due to temperature is a DC drift that would appear from time to time in the data. In figure 6.7 the DC shift is clearly visible at approximately t=1.4E+06 ms. Before and after the resistance shifts, the effects of straining the sample are clearly visible in the resistance plot. This is consistent with the I-V data taken in chapter two where the resistance changes inversely to temperature shown in figure 2.5. Additional tests comparing sensitivity to straining at different temperatures would be interesting to see, as well as tests of these samples though larger ranges of strain.

The driving force behind this research is to develop multifunctional materials, materials that are both load-bearing and self-sensing, which could be integrated in future aerospace vehicles. The findings in this study offer great potential for a variety of aerospace and structural applications. Potential applications include building this device as a stick-on strain monitoring sensor for structural monitoring of buildings, bridges, aircraft, space vehicles and launch vehicles. One specific application that recently has received attention and is being studdied is the use of the extreme small size of the CNTs to fabricate a dense, highly ordered array of CNT strain sensors to be used to map strain fields in localized areas. This idea points immediately to crack growth and crack propagation detection [34].

The aviation industry spends very substantial sums of money inspecting known fatigue locations and already identified cracks to look for crack development, or growth. This practice often includes disassembly of large portions of the aircraft for inspection removes the aircraft from service. This process is labor intensive to perform and incurs the opportunity cost of having the aircraft out of service. Additionally, it is not uncommon to cause additional damage from handling or accidental impacts or other such unforeseen problems by simply taking everything apart and putting it back together. By developing a strain field monitoring sensor, a sensor could be placed in a high fatigue area or over an already known crack and monitored remotely. This could indicate when and even how a crack has developed or grown, by how much and whether or not it is safe to continue operation. The cost benefits in this case are obvious, requiring far less down time of the vehicle or structure, and reducing maintenance costs

and possibilities of real time *in-situ* compensation to prevent further loading of the damaged area leading to catastrophic failure.

7.2 Suggested Future Research

The load testing performed in the study of the flexible polyimide samples concentrated on cyclic tensile testing within a small strain regime. Additional testing would be of interest including strain-to-failure testing, compression testing, and bending mode testing. Each of these tests may reveal properties of the CNT device that could be optimized for future embodiments of the sensor design. Parameters such as preloading, polyimide thickness, and device architecture may be easy parameters to modify, and additional testing would reveal reasons for such considerations.

The empirical data in chapters 2 and 3 suggest a strong correlation to the DEP theory. However, further testing is required to determine exactly if the theoretical prediction accurately predicts preferential alignment of metallic CNTs. Raman spectroscopy is able to discern metallic from semi conducting CNTs deposited on a surface with a high degree of accuracy. Experiments have already made progress towards obtaining this data.

Additionally, further studies are required to improve CNT dispersion and deposition. As described earlier, single tube devices offer fewer unknown variables. Such research is currently underway at NASA Langley Research Center as well as within several other research groups throughout the world. The techniques developed here would directly further the understanding of CNT electro-mechanics by enabling more consistent and reliable fabrication methods and allow for more controlled experiments to determine the CNT sorting potential of DEP.

A CNT deposition study would include investigation into possible ways to deposit single CNTs or single CNT bundles using a more precise methodology. One possibility comes from the literature which indicated the use of a very large series resistor during the dielectrophoresis deposition [14]. This resistor allows a large electric field to exist between the two alignment electrodes during CNT deposition. Once a nanotube or CNT bundle falls into place, it closes the circuit. In doing so, the circuit switches the large voltage drop from between the electrodes to the series resistor. The resistor used in this study was a 100MΩ resistor, a much higher resistance than the contact resistance of a single nanotube. By optimizing such a procedure, it might be possible to have a great deal of control in the deposition of CNTs. By fine tuning the frequency and potential of the alignment, it may also be possible to select specific species, metallic or semiconducting, of CNTs to be aligned. Already, the theoretical calculations made in chapter 2 suggest metallic – semiconductor sorting potential. Futher studies may reveal the ability to sort out individual chiralities of CNTs.

Because of the long and thin aluminum load testing coupons used in this study, compression testing would have been very difficult to perform without inducing buckling. This would require mounting the sensors on a different type of test coupon. Compression testing can be studied in bending mode. However, the samples in the current studies were not designed for this type of testing.

The foundation of this research was to take steps towards the realization of high performance multifunctional materials. This goal has been accomplished through the development of a detailed theory of nanotube positioning and alignment via dielectrophoresis, scanning probe based studies on the strain based conductance change of HiPCO SWCNTs, and finally the fabrication and successful demonstration of a HiPCO SWCNT based strain sensor on

a flexible substrate. With the known strength characteristics of the SWCNTs and the proven strain sensitivity shown in this body of work, we are one step closer to meeting the multifunctional material goal.

References

1. R. Saito, G. Dresselhous, M.S. Dresselhaus, *Physical Properties of Carbon Nanotubes*. Imperial College Press, 2001.

2. M.S. Dresselhaus, G. Dresselhaus, P. Avouris, *Carbon Nanotubes, Synthesis, Structure, Properties, and Applications.* Springer, 2001.

3. Nanotubes obtained from Carbon Nanotechnologies, Inc. 16200 Park Row, Houston, TX 77084-5195.

4. M. Bronikowski, P. Willis, D. Colbert, K. Smith, R. Smalley, "Gas-Phase Production of Carbon Single-Walled Nanotubes from Carbon Monoxide via the HiPco Process: a Parametric Study." *Journal of Vacuum Science & Technology: A - Vacuum Surfaces & Films,* Vol.19, No. 4, 2001, pp. 1800-1805.

5. I. W. Chiang, B. E. Brinson, A. Y. Huang, P. A. Willis, M. J. Brownikowski, J. L. Margrave, R. E. Smalley and R. H. Hauge. "Purification and Characterization of Single-Wall Carbon Nanotubes (SWNTs) Obtained from the Gas-Phase Decomposition of CO (HiPco Process)." *Journal of Physical Chemistry: B*, Vol. 105, 2001, pp. 8297-8301.

6. J. Smits, B. Wincheski, M. Namkung, R. Crooks, R. Louie, "Response of Fe Powder, Purified and As-Produced HiPco Single-Walled Carbon Nanotubes to Flash Exposure," *Materials Science and Engineering: A*, Vol. A358, 2003, pp. 384-389.

7. E.D. Minot, Y. Yaish, Sazonova, J. Park, M. Brink, P.l. McEuen, "Tuning Carbon Nanotube Bandgaps with Strain," *Physical Review Letters*, Vol. 90, No. 15, 2003, pp. 156401-1 - 156401-4.

8. J. Cao, Q. Wang, H. Dai. "Electromechanical Properties of Metallic, Quasimetallic, and Semiconducting Carbon Nanotubes under Stretching." *Physical Review Letters,* Vol. 90, No. 15, 2003, pp. 157601-1 - 157601-4.

9. T. W. Tombler, C. Zhou, L. Alexseyev, J. Kong, H. Dai, L. Liu, C. S. Jayanthi, M. Tang, S. Wu, "Reversible Electromechanical Characteristics of Carbon Nanotubes under Local-Probe Manipulation," *Nature*, Vol. 405, 2000, pp. 769-772.

10. J. Smits, B. Wincheski, J. Ingram, N. Watkins, J. Jordan. "Controlled Deposition and Applied Field Alignment of Single Walled Carbon Nanotubes for CNT Device Fabrication," *Materials Research Society Symposium Proceedings,* Vol. 739, 2002, pp. h7.11.1 - h7.11.6.

11. L. X. Benedict, S. G. Louie, M. L. Cohen, "Static Polarizabilities of Single-Wall Carbon Nanotubes." *Physical Review: B*, Vol. 52, No. 11, 1995, pp. 8541-8549.

12. B. Wincheski, M. Namkung, J. Smits, P. Williams, R. Harvey, “Effect of Alignment on Transport Properties of Carbon Nanotube/Metallic Junctions” *Materials Research Society Symposium proceedings,* Vol. 772, 2003, pp. M9.2.1 - M9.2.6.

13. F. Wakaya, T. Nagai, K. Gamo, “Position Control of Carbon Nanotube using Patterned Electrode and Electric Field.” *Microelectronic Engineering,* Vol. 63, 2002, pp. 27-31.

14. R. Krupke, F.Hennrich, H.B. Weber, D. Beckmann, O. Hampe, S.Malik, M.M. Kappes, H.V. Lohneysen, “ Contacting Single Bundles of Carbon Nanotubes with Alternating Electric Fields.” *Applied Physics: A,* Vol. 76, 2003, pp. 397-400.

15. L.A. Nagahara, I. Amlani, J. Lewenstein, R. Tsui, “Direct Placement of Suspended Carbon Nanotubes for Nanometer-Scale Assembly.” *Applied Physics Letters*, Vol. 80, No. 20, 2002, pp. 3826-3827.

16. H. A. Pohl, *Dielectrophoresis, the Behavior of Neutral Matter in Nonuniform Fields,* Cambridge University Press, 1978.

17. J.D. Jackson, *Classical Electrodynamics*, John Wiley and Sons, Inc., 1962.

18. N.W. Ashcroft, N.D. Mermin, *Solid State Physics,* Saunders College Publishing, 1976.

19. D.A. Walters, M.J. Casavant, X.C. Qin, C.B. Huffman, P.J. Boul, L.M. Ericson, E.H.Haroz, M.J. O’Connell, K. Smith, D.T. Colbert, R.E. Smalley, “In-Plane-Alligned Membranes of Carbon Nanotubes,” *Chemical Physics Letters*, Vol. 388, 2001, pp. 14-20.

20. R. Heyd, A. Charlier, E. McRae, “Uniaxial-Stress Effects on the Electronic Properties of Carbon Nanotubes” *Physical Review: B*, Vol. 55, 1997, pp. 6820-6824.

21. M. Bockrath, D. H. Cobden, P. L. McEuen, N. G. Chopra, A.Zettl, A. Thess, R. E. Smalley, “Single-Electron Transport in Ropes of Carbon Nanotubes.” *Science*, Vol. 275, 1997, pp. 1922-1925.

22. J McMurry, R. Fay, *Chemistry*, 2nd edition, Prentice Hall, 1998.

23. V. C. Moore, M. S. Strano, E. H. Haroz, R. H. Hauge, R. E. Smalley, "Individually suspended single-walled carbon nanotubes in various surfactants." *Nano Letters*, Vol. 3, No. 10, 2003, pp. 1379-1382.

24. M. F. Islam, E. Rojas, D. M. Bergey, A. T. Johnson, A.G. Yodh, "High weight fraction surfactant solubilization of single-wall carbon nanotubes in water." *Nano Letters,* Vol. 3, No. 2, 2003, pp. 269-273.

25. C. A. Dyke, J. M. Tour. "Unbundled and highly functionalized carbon nanotubes from aqueous reactions." *Nano Letters,* Vol. 3, No. 9, 2003, pp. 1215 -1218.

26. R. Louie, R. Wincheski, M. Namkung, J. Smits, *personal communication*, (presentation to NASA Langley Research Center, Nondestructive Evaluation Sciences Branch, July, 2002).

27. M.R. Falvo, G. Clary, A. Helser, S. Paulson, R.M. Taylor II, V. Chi, F.P. Brooks, Jr., S. Washburn, and R. Superfine, "Nanomanipulation Experiments Exploring Frictional and Mechanical Properties of Carbon Nanotubes," *Microscopy and Microanal*ysis, Vol. 4, 1999, pp. 504-512.

28. M. Guthold, M. R. Falvo, W. G. Matthews, S. Paulson, S. Washburn, D. A. Erie, R. Superfine, F. P. Brooks Jr., R. M. Taylor, II., "Controlled Manipulation of Molecular Samples with the nanoManipulatior," *IEEE/ASME Transactions on Mechatronics*, Vol. 5, Issue: 2 , June 2000, pp. 189 – 198.

29. J. Liu, M. J. Casavant, M. Cox, D.A. Walters, P. Boul, W. Lu, A. J. Rimberg, K. A. Smith, D. T. Colbert, R. E. Smalley, "Controlled Deposition of Individual Single-Walled Carbon Nanotubes on Chemically Functionalized Templates," *Chemical Physics Letters*, Vol. 303, 2000, pp. 125-129.

30. K. H. Choi, J. P. Bourgoin, S. Auvray, D. Esteve, G. S. Duesberg, S. Roth, M. Burghard, "Controlled Deposition of Carbon Nanotubes on a Patterned Substrate," *Surface Science*, Vol. 462, 1999, pp. 195-202.

31. B. Wincheski, J. Smits, M. Namkung, J. Jordan, and R. Louie "Nanomanipulation and Lithography for Carbon Nanotube Based Nondestructive Evaluation Sensor Development," *Proceedings of the 2002 SEM Conference on Experimental Mechanics*, 2002.

32. J. Smits, B. Wincheski, J.L. Ingram, A.N. Watkins, and J.D. Jordan, "Method for the Controlled Deposition and Alignment of Single Walled Carbon Nanotube," US Patent application, NASA Case No. LAR-16499-1, 2002.

33. J. Smits, B. Wincheski, J. Ingram, A. N. Watkins, J. Jordan, P. Williams, "Single Wall Carbon Nanotube-Based Structural Health Sensing Materials," *Technical Proceedings of the 2004 NSTI Nanotechnology Conference and Trade Show*, Vol. 3, 2004, pp. 149-152.

34. J. Smits, T. Moore, B. Wincheski, J. Ingram, N. Watkins, P. Williams and T. Kite, "CNT based crack growth detector and strain field monitor." Invention Disclosure, NASA Langley Case No. LAR-16900-1, 2004.

REPORT DOCUMENTATION PAGE

Form Approved
OMB No. 0704-0188

1. REPORT DATE *(DD-MM-YYYY)*	2. REPORT TYPE	3. DATES COVERED *(From - To)*
01- 07 - 2005	Contractor Report	

4. TITLE AND SUBTITLE

Strain Sensitivity in Single Walled Carbon Nanotubes for Multifunctional Materials

5a. CONTRACT NUMBER

NAS1-00135

5b. GRANT NUMBER

5c. PROGRAM ELEMENT NUMBER

6. AUTHOR(S)

Smits, Jan M., VI

5d. PROJECT NUMBER

5e. TASK NUMBER

5f. WORK UNIT NUMBER

FC400000

7. PERFORMING ORGANIZATION NAME(S) AND ADDRESS(ES)

NASA Langley Research Center
Hampton, VA 23681-2199

Swales Aerospace
Hampton, VA 23666

8. PERFORMING ORGANIZATION REPORT NUMBER

9. SPONSORING/MONITORING AGENCY NAME(S) AND ADDRESS(ES)

National Aeronautics and Space Administration
Washington, DC 20546-0001

10. SPONSOR/MONITOR'S ACRONYM(S)

NASA

11. SPONSOR/MONITOR'S REPORT NUMBER(S)

NASA/CR-2005-213272

12. DISTRIBUTION/AVAILABILITY STATEMENT

Unclassified - Unlimited
Subject Category 70
Availability: NASA CASI (301) 621-0390

13. SUPPLEMENTARY NOTES

Thesis to the Faculty of the School of Engineering and Applied Science, The George Washington University, in partial fulfillment of the requirements for the Degree of Master of Science, Aug. 31, 2004. Langley Technical Monitor: D. M. Heath
An electronic version can be found at http://ntrs.nasa.gov

14. ABSTRACT

Single walled carbon nanotubes represent the future of structural aerospace vehicle systems due to their unparalleled strength characteristics and demonstrated multifunctionality. This multifunctionality rises from the CNT's unique capabilities for both metallic and semiconducting electron transport, electron spin polarizability, and band gap modulation under strain. By incorporating the use of electric field alignment and various lithography techniques, a single wall carbon nanotube (SWNT) test bed for measurement of conductivity/strain relationships has been developed. Nanotubes are deposited at specified locations through dielectrophoresis. The circuit is designed such that the central, current carrying section of the nanotube is exposed to enable atomic force microscopy and manipulation *in situ* while the transport properties of the junction are monitored. By applying this methodology to sensor development a flexible single wall carbon nanotube (SWNT) based strain sensitive device has been developed. Studies of tensile testing of the flexible SWNT device vs conductivity are also presented, demonstrating the feasibility of using single walled HiPCO (high-pressure carbon monoxide) carbon nanotubes as strain sensing agents in a multi-functional materials system.

15. SUBJECT TERMS

Carbon; Nanotubes; Strain

16. SECURITY CLASSIFICATION OF:			17. LIMITATION OF ABSTRACT	18. NUMBER OF PAGES	19a. NAME OF RESPONSIBLE PERSON
a. REPORT	b. ABSTRACT	c. THIS PAGE			STI Help Desk (email: help@sti.nasa.gov)
					19b. TELEPHONE NUMBER *(Include area code)*
U	U	U	UU	97	(301) 621-0390